

**UNCLASSIFIED**

**AD 408 755**

---

**DEFENSE DOCUMENTATION CENTER**

**FOR**

**SCIENTIFIC AND TECHNICAL INFORMATION**

**CAMERON STATION, ALEXANDRIA, VIRGINIA**



**UNCLASSIFIED**

NOTICE: When government or other drawings, specifications or other data are used for any purpose other than in connection with a definitely related government procurement operation, the U. S. Government thereby incurs no responsibility, nor any obligation whatsoever; and the fact that the Government may have formulated, furnished, or in any way supplied the said drawings, specifications, or other data is not to be regarded by implication or otherwise as in any manner licensing the holder or any other person or corporation, or conveying any rights or permission to manufacture, use or sell any patented invention that may in any way be related thereto.

408 755

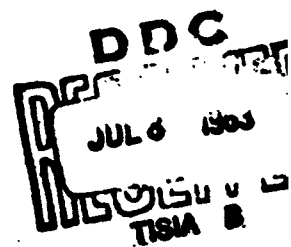
63-42

19

CATALOGED BY DDC  
AS AD No. 408755



**HERCULES**



CHEMICAL PROPULSION DIVISION  
**HERCULES POWDER COMPANY**  
INCORPORATED  
BACCHUS WORKS MAGNA, UTAH

Technical Operating Report

B O B Approval No.

Contract Number AF 04(647)-243  
Exhibit B Volume 1 Section 3  
Paragraph 4.2.3.5

A METHOD OF OBTAINING AN OVERALL  
HEAT TRANSFER FILM COEFFICIENT  
IN SOLID FUEL ROCKET NOZZLES

WEAPON SYSTEM 133A

May 1963

Prepared by

HERCULES POWDER COMPANY  
CHEMICAL PROPULSION DIVISION  
Bacchus Works  
Magna, Utah

Prepared for

HEADQUARTERS  
AIR FORCE SYSTEMS COMMAND  
UNITED STATES AIR FORCE  
Los Angeles, California

Report No. \_\_\_\_\_


Copy No. 19

Date 7 May 1963

A METHOD OF OBTAINING AN OVERALL  
HEAT TRANSFER FILM COEFFICIENT  
IN SOLID FUEL ROCKET NOZZLES


WEAPON SYSTEM 133A

Approved by

  
A. H. Peterson, Supervisor  
Advanced Rocket Design

  
D. E. Boynton, Superintendent  
Advanced Development

Prepared by

  
J. W. Lindsey, Engineer  
Advanced Rocket Design

  
W. L. Gunter  
Minuteman Project Manager

## FOREWORD

This report was prepared by the Advanced Rocket Design Group of Hercules Powder Company at Bacchus, Utah. The information contained in this report was obtained to demonstrate the feasibility of an experimental and theoretical technique for determining temperatures and heat transfer film coefficients in rocket nozzles. The technique presented here is intended to be one by which the design engineer can more easily properly design a rocket nozzle from a set of measured or assumed nozzle wall temperatures.

## SUMMARY

It is common practice to design solid fuel rocket nozzles (from a thermal standpoint) by applying some constant multiplying factor to the heat transfer convective film coefficient. This multiplying factor is supposed to take care of the heat received by the nozzle due to radiation, dissociation, recombination, and particle impingement. The unfortunate part of this technique is that the safety factor used is arrived at by raising the factor after each nozzle failure until a successful firing is realized. This process is usually a very expensive one in both time and money. An additional expense is encountered since a safety factor is usually found for the nozzle throat while the rest of the nozzle is left overdesigned.

To circumvent this problem a method was needed to determine an overall or total film coefficient that could be used by a nozzle design engineer. Both the experimental technique and the data analysis should be relatively simple to speed their use as design tools.

A method is proposed whereby special ablative thermocouples are used to record the inside surface temperatures of a nozzle during firing. The recorded temperatures are then used as boundary conditions for a transient wall temperature equation. The equation is then solved for the total film coefficient. The solution is an iterative one that requires making an estimate of the film coefficient and using it to calculate a better one. The calculated value is then used to find a third value and so on until the calculated value ceases to vary beyond some set limit.

For the particular tests performed in this study, the film coefficient was seen to be a strong function of time for the first five seconds of firing. Calculated film coefficient values were reduced in some cases by

as much as 40% during the one second to five second interval. Particularly for the first few seconds of firing the film coefficient values as calculated from the method presented in this report are found to be considerably higher than those being predicted by purely convective methods.



## TABLE OF CONTENTS

Foreword - - - - -	i
Summary - - - - -	ii
Table of Contents - - - - -	iv
List of Illustrations - - - - -	v
List of Symbols - - - - -	vii
Introduction - - - - -	1
Objectives - - - - -	3
Experiment Design - - - - -	4
Test Results and Analysis - - - - -	8
Conclusions and Recommendations - - - - -	25
List of References - - - - -	70

# LIST OF ILLUSTRATIONS

<u>Figure No.</u>	<u>Title</u>	<u>Page No.</u>
1	Nanmac Model "P" Thermocouple	27
2a, b, c	Thermocouple Installation Drawing	28, 29a, 29b
3	First Test Motor with Nozzle Prior to Firing	30
4	Second Test Motor with Nozzle Prior to Firing	31
5	Thermocouple to Instrument House Circuit	32
6	HTC D-2 After Firing	33
7	HTC D-2 After Firing	34
8	HTC D-3 After Firing	35
9	HTC D-3 After Firing	36
10	Instrumented Nozzle After Firing	37
11	Instrumented Nozzle After Firing	38
12	Instrumented Nozzle After Firing	39
13	Instrumented Nozzle After Firing	40
14	Instrumented Nozzle After Firing	41
15	Broken Thermocouples	42
16	Thermocouple 11-2 Showing Loss of Inside Core	43
17	Gas Leak Around TC 11-4	44
18	Gas Leak Around TC 11-8	45
19	Erosion Around TC 11-4	46
20	Erosion Around TC 11-8	47
21	Physical Model of Analysis	9
22	Area vs. Radius	11
23	Thermal Properties of High Density Carbon	48
24	Integrated Average Thermal Properties of High Density Carbon	49

LIST OF ILLUSTRATIONS (cont'd)

<u>Figure No.</u>	<u>Title</u>	<u>Page No.</u>
25	Film Coefficient vs Time	50
26	Film Coefficient vs Nozzle Position	51
27	Temperature Plot, TC 11-2	52
28	Temperature Plot, TC 11-3	53
29	Temperature Plot, TC 11-4	54
30	Temperature Plot, TC 11-5	55
31	Temperature Plot, TC 11-6	56
32	Temperature Plot, TC 11-7	57
33	Temperature Plot, TC 11-8	58
34	Temperature Plot, TC 11-9	59
35	Temperature Plot, TC 11-11	60
36	Temperature Plot, TC 51	61
37	Temperature Plot, TC 52	62
38	Temperature Plot, TC 54	63
39	Temperature Plot, TC 55	64
40	Temperature Plot, TC 56	65
41	Temperature Plot, TC 57	66
42	Temperature Plot, TC 58	67
43	Temperature Plot, TC 59	68
44	Temperature Plot, TC 60	69

# LIST OF SYMBOLS

$q$	= Heat Flux - BTU/HR
$K$	= Heat Conductivity - BTU/FT-Hr-°F
$A$	= Area - FT <sup>2</sup>
$T$	= Temperature - °R
$r$	= Radius - FT
$c$	= Heat Capacity - BTU/(LB - °F)
$\rho$	= Density - LBS/FT <sup>3</sup>
$L$	= Unit Length - FT
$\alpha$	= Thermal Diffusivity - FT <sup>2</sup> /Hr
$P$	= Heavisides Operator - $\frac{\partial}{\partial t}$
$B$	= Area Constant - 1/FT
$j$	= $\sqrt{-1}$
$T_w$	= Wall Temperature - °R
$T_g$	= Gas Static Temperature - °R
$R_o$	= Outside Radius - FT
$R_i$	= Inside Radius - FT
$h$	= Heat Transfer Film Coefficient BTU/(HR-FT <sup>2</sup> -°F)
$D_*$	= Throat Diameter - IN
$\mu$	= Viscosity - LB/IN-SEC
$C_p$	= Specific Heat - BTU/LB-°F
$Pr$	= Prandtl Number - Dimensionless
$P_c$	= Chamber Pressure - LBS/IN <sup>2</sup> Abs.
$g$	= Gravitational Acceleration - FT/SEC <sup>2</sup>
$C^*$	= Characteristic Velocity - FT/SEC
$A_*$	= Throat Area - IN <sup>2</sup>

$\dot{m}$  = Mass Flow Rate - LBM/SEC  
 $r_c$  = Radius of Curvature - IN  
 $\omega$  = Exponent - Dimensionless  
 $M$  = Mach Number - Dimensionless  
 $\gamma$  = Ratio of Specific Heats - Dimensionless  
 $T_o$  = Stagnation Temperature -  $^{\circ}R$

## INTRODUCTION

The rapid development of the present generation of solid fuel missiles is largely due to the ability of those engineers and scientists doing the developing to select and discard design ideas purely on the basis of past experience or intuition. Unfortunately the past experience and intuitive ideas of most people were gained by working in lower temperature ranges than those encountered in solid fuel rocketry, especially the temperatures developed by modern propellants with metal additives.

The one area of rocket design that has probably suffered the most from high temperatures inexperience is nozzle construction. Coupled with the requirement that nozzle materials withstand high temperatures are the additional requirements that the nozzle assembly be as light as possible and still be highly resistant to thermal shock and dimensional changes due to erosion and thermal expansion. These requirements in themselves do not seem to present very difficult design problems on the surface until the designing engineer takes down his heat transfer text book and decides to look at transient temperature distributions in his particular nozzle. One of the first stumbling blocks the designer must overcome is to find a way to predict reasonable values of a convective film coefficient for the case of a chemically reacting gas where dissociation and recombination are occurring in the boundary layer.

The problem of heat flux to the nozzle wall is further complicated by the metal additive in the propellant that leaves the motor combustion chamber as tiny droplets of molten oxide. These metal particles apparently have no regard for a boundary layer and impinge upon the nozzle wall, usually to be carried immediately downstream. An even more serious effect of the particles

is the heat transferred to the nozzle by radiation. At the present time it is very difficult to account for the radiation component of heat because of a lack of information dealing with particle size, distribution, and temperature.

Unable to account for the dissociation, recombination, impingement, and radiation in the nozzle environment the designing engineer usually resigns himself to calculating a convective film coefficient based on fully developed turbulent flow. A safety factor is then multiplied by the resulting answer with the magnitude of the safety factor dependent on how vividly the engineer recalls the previous failures of similar designs where lower safety factors were used.

This technique will obviously lead eventually to a successful nozzle design program. It will do so however with a nozzle that is at least slightly overdesigned and very likely well overdesigned in local areas. This technique will also shed very little light on the radiation heat transfer or how to account for it. The design of rocket nozzles thus becomes more and more an art and less and less a science. While a certain amount of art is always justified it cannot be relied upon in a final analysis or a design optimization.

A thorough investigation of the heat received by a nozzle during a rocket firing must wait until more information becomes available on chemically reactive boundary layers and on the behavior and effects of metal oxide particles. It would be well at this time however to record the temperatures actually found on a nozzle wall and from them deduce a value of an overall film coefficient. This would then be compared with convective film coefficients predicted by present methods.

## OBJECTIVES

The objectives of this study are as follows:

1. Design and conduct an experiment to record the flow surface wall temperatures developed in a rocket nozzle during firing.
2. Develop a transient mathematical model for the nozzle wall temperatures.
3. Use the recorded wall temperatures in the mathematical model to solve for an overall film coefficient.
4. Compare the overall coefficient with a pure convective film coefficient.



## EXPERIMENT DESIGN

At the time of this study the nozzle of prime interest was the nozzle used on the third stage of the Minuteman Missile. It was therefore, decided to perform the experiment directly on that nozzle. The cost of firing a third stage Minuteman motor is excessive so the decision was made to fire an experimental nozzle on a smaller, one nozzle test motor. This test motor was called a half-ton charge (HTC) and with it's single nozzle configuration would subject the nozzle to less severe punishment than would the four-nozzle Minuteman. If the firing proved successful, the experiment would be repeated later on a Minuteman full-size unit (FSU).

To successfully and accurately record the nozzle wall temperatures the sensing elements used should be able to withstand the effects of the gas flow and temperature at least as well as the nozzle material in the area being investigated. If a thermocouple type device were used, it should be mounted flush with the nozzle wall to eliminate the possibility of measuring gas stagnation temperature instead of wall surface temperature. The recording element cross sectional area should be a minimum to reduce conduction error along the element and increase the time response. In view of the fact that the nozzle wall erodes during firing the sensing element should also erode and give continuous readings during the erosion process.

A special eroding thermocouple produced by the Nanmac Corporation, Indian Head, Maryland was found to fill all of the requirements listed above. The Nanmac model "P" thermocouple has the unique feature of having the body of the thermocouple fabricated of the same material as that being investigated; therefore matching ablation and conduction exactly in the thermocouple

body. The sensing element consists of a very fine Tungsten strip separated from a Tungsten - 26% Rhenium strip by a very thin spacer of mica as shown in Figure 1. When the threaded thermocouple is screwed into its threaded hole until it projects slightly a lock nut secures the thermocouple for the test. The projecting tip of the thermocouple is then sanded flush to the nozzle wall. The sanding operation establishes the initial contact between the two metal strips. With careful polishing of the tip the time response can be brought as low as ten micro-seconds.

The thermocouples were arranged to show the variation of wall surface temperature throughout the length of the nozzle. In the expansion cone of the nozzle duplicate thermocouples were installed diametrically opposite to one another. Iron-constantan thermocouples were used to monitor the junction of the lead in wires to the thermocouple. The placement of the thermocouples is shown in Figure 2 along with the instructions for installation.

The fully instrumented nozzle is shown on the test engine before firing in Figures 3 and 4. Note that the thermocouples are shielded with an insulating potting compound and all cables are asbestos wrapped. All wiring is then wrapped with aluminum foil.

Range instrumentation procedures require that three patch boards be included in the circuit between the thermocouples and the recording instruments. This is shown schematically, in Figure 5, with the type of lead wires used for each portion of the circuit.

During the instrumentation of the nozzle two of the carbon based thermocouples were broken. Because of the fragile behavior of the thermocouples and the high cost of each (\$175/ea for carbon base, \$125/ea for phenolic base) it was decided to delay the installation until the motor

was in the firing bay. This would eliminate possible breakage during handling of the motor.

With all of the thermocouples installed the first motor was finally fired on 4 May 1962 and the second on 25 March 1963. Various views of the motors immediately after firing are shown in Figures 6, 7, 8, and 9. The detached nozzle is shown in Figures 10, 11, 12, 13, and 14.

#### First Test:

When the insulating shielding was stripped from the thermocouples after firing, unit 11-1 fell free of the nozzle while 11-2 was broken but not separated. This condition is shown in Figure 15. The inside core was missing from thermocouple 11-2 as shown in Figure 16. It is believed that the core was not lost until after the test when the surface began cooling and the pressure dropped. A small amount of gas trapped in the thermocouple body probably pushed the core out when the motor pressure dropped low enough to permit it.

Thermocouples 11-4 and 11-8 developed slight gas leaks around their bases as evidenced in Figures 17 and 18. This condition apparently did not interfere seriously with their operation.

All thermocouples located in the exit cone survived the firing exceptionally well. Some erosion was observed around 11-4 and 11-8 as shown in Figures 19 and 20. For this reason the data from these thermocouples should not be taken as being very exact late in the firing. Temperatures and flow conditions in the phenolic exit cone do not appear severe enough to keep the tungsten elements burned off level with the surface. Subsequent testing should probably use platinum-rhodium thermocouples. Since the tips were not kept flush they protruded into the gas stream and did not record the wall surface temperatures after about the first quarter of firing.

Second Test:

Detailed photographs of the second test nozzle were not obtained after firing. Visual inspection showed thermocouples 51, 52, and 53 to be in very good condition with only very slight erosion around the sensing tip. Thermocouples 54 and 57 were eroded below the surface of the surrounding material. Thermocouple 54 had a large metallic bead at the junction that protruded out into the flow stream. All of the phenolic thermocouples in the exit cone were eroded approximately 1/16 inch below the surface of the surrounding material.

Considering this was the first time thermocouples of this type have been used at the Hercules, Bacchus range and the first time ever to be used on a rocket motor with combustion temperatures in excess of 6500°R the firing is to be considered a complete success with exceptionally good data.

## TEST RESULTS AND ANALYSIS

Data were not obtained on thermocouples 11-1 and 11-10 on the first test and thermocouple 53 on the second test due to the last minute development of circuit problems either in the thermocouples themselves or the channels used to record the data.

During the firing a millivolt output from each thermocouple was recorded by visicorder and digital tape. The digital tape data was then converted to temperatures through the use of the thermocouple manufacturers' conversion table. The converted temperatures are given in Figures 27 through 35 for the first firing and Figures 36 through 44 for the second firing.

Considerable deviation in the readings is observed after about ten seconds of firing. It is felt that these deviations are due to erosion around the thermocouple tips, tips protruding into the flow stream and other similar developments. For this reason only the data from the first ten seconds will be used in the following analysis. This should pose no great restriction since most of the thermocouples leveled off at about this time.

In the development of the mathematical model to be used in analyzing the data the following simplifications or assumptions are made.

1. The thermal properties of the nozzle materials are not temperature dependent.
2. The flow channel at any point of investigation is a simple cylinder with parallel walls.
3. The nozzle wall is composed of a single non-ablating homogeneous material.
4. The temperature inside the nozzle wall at some radius,  $R_0$ , remains at the original ambient temperature.

It is argued that these simplifications were used for the following reasons:

1. The first assumption is justified on the grounds that while it is well known that present nozzle materials have temperature dependent thermal properties it is difficult to include the dependency in the equations. Integrated averages will therefore be used in this analysis after the mathematical model has been formulated.

2. The second assumption is to reduce the computations required to allow the channel cross-section to vary. The solution being sought is a point solution anyway and should be independent of an axial length parameter in the nozzle.

3. The nozzle areas of prime interest in this analysis are the nozzle approach or inlet and the throat region. Since these areas are presently fabricated of a thick layer of high density graphite, assumption 3 is assumed to be valid.

4. The ten second limitation on the data is considered a strong justification of assumption 4. The outside radius,  $R_o$ , is taken as the outside dimension of the high density graphite.

Other limitations or simplifications are discussed as the mathematical model is developed.

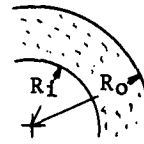


Figure 21, Physical Model of Analysis

Heat conduction:

$$q = -KA \frac{\partial T}{\partial r} \quad (1)$$

Heat balance:

$$\frac{\partial q dr}{\partial r} = -c\rho A dr \frac{\partial T}{\partial t} \quad (2)$$

$$-K \left[ A \frac{\partial^2 T}{\partial r^2} + \frac{\partial T}{\partial r} \frac{\partial A}{\partial r} \right] = -c\rho A dr \frac{\partial T}{\partial t} \quad (3)$$

$$\frac{\partial^2 T}{\partial r^2} + \frac{1}{A} \frac{\partial A}{\partial r} \frac{\partial T}{\partial r} = \frac{c\rho}{K} \frac{\partial T}{\partial t} \quad (4)$$

Using Heavisides notation from operational calculus and denoting  $\frac{K}{c\rho}$  as  $\alpha$ ,

$$\frac{\partial T}{\partial r} + \frac{1}{A} \frac{\partial A}{\partial r} \frac{\partial T}{\partial r} = \frac{P}{\alpha} \quad (5)$$

This equation is difficult to solve in its present form but would be much easier if we could say

$$\frac{1}{A} \frac{\partial A}{\partial r} = B = \text{constant} \quad (6)$$

$$\ln |A| \Big|_{A_1}^{A_0} = rB \Big|_{R_1}^{R_0} \quad (7)$$

$$\ln 2\pi R_0 L - \ln 2\pi R_1 L = B (R_0 - R_1) \quad (8)$$

$$B = \frac{\ln (R_0/R_1)}{(R_0 - R_1)} \quad (9)$$

This statement amounts to having the area vary exponentially with the radius rather than linearly with it.

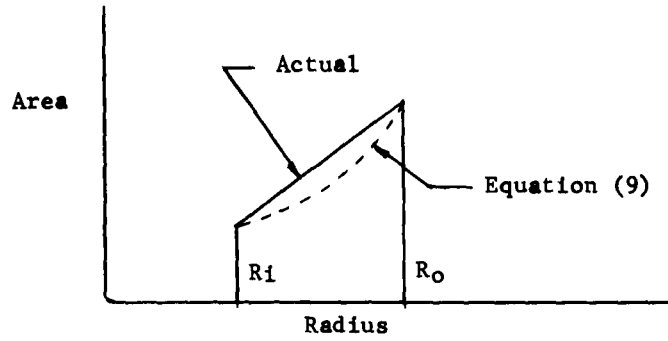


Figure 22, Area vs Radius

$$(9) \longrightarrow (15) \quad \frac{\partial^2 T}{\partial r^2} + B \frac{\partial T}{\partial r} = \frac{P}{\alpha} \quad (10)$$

$$\text{or} \quad m^2 + Bm = \frac{P}{\alpha} \quad (11)$$

$$\text{therefore} \quad m = -\frac{B}{2} \pm j \sqrt{-\left(\frac{B}{2}\right)^2 - \frac{P}{\alpha}} \quad (12)$$

$$m = -\frac{B}{2} \pm j E \quad (13)$$

$$\text{where} \quad E = \sqrt{-\left(\frac{B}{2}\right)^2 - \frac{P}{\alpha}} \quad (14)$$

The solution to (10) then becomes

$$T = e^{-\frac{Br}{2}} \left[ \theta \cos Er + \phi \sin Er \right] \quad (15)$$

Where  $\theta$  and  $\phi$  are constants of integration.

$$(15) \longrightarrow (1)$$

$$q = -KAe^{-\frac{Br}{2}} \left[ \theta(-E \sin Er - \frac{B}{2} \cos Er) + \phi(E \cos Er - \frac{B}{2} \sin Er) \right] \quad (16)$$

Now at  $r = R_1$ ,  $T = T_w$  and  $q = 2\pi R_1 L h (T_g - T_w)$  or

$$T_w = e^{-\frac{BR_1}{2}} \left[ \theta \cos ER_1 + \phi \sin ER_1 \right] \quad (17)$$

$$\text{and } q = h2\pi R_1 L \left[ T_g - e^{-\frac{BR_1}{2}} (\theta \cos ER_1 + \phi \sin ER_1) \right] \quad (18)$$



(18)  $\longrightarrow$  (16) at  $r = R_1$

$$h (T_g - e^{-\frac{BR_1}{2}} \left[ \theta \cos ER_1 + \phi \sin ER_1 \right]) =$$

$$- K e^{-\frac{BR_1}{2}} \left[ \theta (-E \sin ER_1 - \frac{B}{2} \cos ER_1) + \phi (E \cos ER_1 - \frac{B}{2} \sin ER_1) \right] \quad (19)$$

For the second boundary condition we say that at  $r = R_0$ ,  $T = T_a = 0$  where the ambient temperature,  $T_a$ , will be used as a reference temperature and can therefore be considered as a zero temperature.

$$0 = e^{-\frac{BR_0}{2}} \left[ \theta \cos ER_0 + \phi \sin ER_0 \right] \quad (20)$$

Simultaneous solution of (19) and 20) yields:

$$\phi = \frac{-\frac{h}{k} T_g e^{\frac{BR_1}{2}}}{\sin ER_1 (E \tan ER_0 - \frac{B}{2} - \frac{h}{k}) + \cos ER_1 (\frac{B}{2} \tan ER_0 + \frac{h}{k} \tan ER_0 + E)} \quad (21)$$

$$\theta = \frac{-\frac{h}{k} T_g e^{\frac{BR_1}{2}} \tan ER_0}{\sin ER_1 (E \tan ER_0 - \frac{B}{2} - \frac{h}{k}) + \cos ER_1 (\frac{B}{2} \tan ER_0 + \frac{h}{k} \tan ER_0 + E)} \quad (22)$$

(21), (22)  $\longrightarrow$  (15)

$$T = \frac{\frac{h}{k} T_g e^{\frac{B}{2} (R_1 - r)} (\tan ER_0 \cos ER_1 - \sin ER_1)}{\sin ER_1 (E \tan ER_0 - \frac{B}{2} - \frac{h}{k}) + \cos ER_1 (\frac{B}{2} \tan ER_0 + \frac{h}{k} \tan ER_0 + E)} \quad (23)$$

Now at  $r = R_1$   $T = T_w$

$$T_w = \frac{\frac{h}{k} T_g (\tan ER_0 \cos ER_1 - \sin ER_1)}{\sin ER_1 (E \tan ER_0 - \frac{B}{2} - \frac{h}{k}) + \cos ER_1 (\frac{B}{2} \tan ER_0 + \frac{h}{k} \tan ER_0 + E)} \quad (24)$$

Dividing numerator and denominator by  $\cos E$ , equation (21) reduces to:

$$T_w = \frac{\frac{h}{k} T_g \sin [E(R_0 - R_1)]}{E \cos [E(R_0 - R_1)] + \left(\frac{B}{2} + \frac{h}{k}\right) \sin [E(R_0 - R_1)]} \quad (25)$$

Now by Heavisides operational calculus methods equation (25) must be further integrated in time.

$$T_w = \frac{Y(0)}{Z(0)} + \sum_{n=0}^{\infty} \frac{Y(p)}{p} \frac{e^{pt}}{\frac{Z(p)}{dp}} \quad (26)$$

where  $\frac{Y(0)}{Z(0)}$  is the steady state

solution obtained by letting  $p=0$  in

$$Y(p) = \frac{h}{k} T_g \sin [E(R_0 - R_1)] \quad (27)$$

$$\text{and } Z(p) = E \cos [E(R_0 - R_1)] + \left(\frac{B}{2} + \frac{h}{k}\right) \sin [E(R_0 - R_1)] \quad (28)$$

Setting  $p=0$  in (14),  $E = \frac{jB}{2}$

$$\frac{Y(0)}{Z(0)} = \frac{\frac{h}{k} T_g \sin \left[ \frac{jB}{2} (R_0 - R_1) \right]}{\frac{jB}{2} \cos \left[ \frac{jB}{2} (R_0 - R_1) \right] + \left(\frac{B}{2} + \frac{h}{k}\right) \sin \left[ \frac{jB}{2} (R_0 - R_1) \right]} \quad (29)$$

$$= \frac{\frac{h}{k} T_g}{\frac{h}{k} + \frac{B}{2} (1 + \coth \left[ \frac{B}{2} (R_0 - R_1) \right])} \quad (30)$$

(9)  $\rightarrow$  (30)

$$\frac{Y(0)}{Z(0)} = \frac{\frac{h}{k} T_g}{\frac{h}{k} + \frac{\ln (R_0/R_1)}{2 (R_0 - R_1)} \left( 1 + \frac{(R_0/R_1)^{\frac{1}{2}} + (R_0/R_1)^{-\frac{1}{2}}}{(R_0/R_1)^{\frac{1}{2}} - (R_0/R_1)^{-\frac{1}{2}}} \right)} \quad (31)$$

$$= \frac{\frac{h}{k} T_g}{\frac{h}{k} + \frac{\ln (R_0/R_1)}{2 (R_0 - R_1)} \left( 1 + \frac{R_0/R_1 + 1}{R_0/R_1 - 1} \right)} \quad (32)$$

$$\frac{Y(0)}{Z(0)} = \frac{\frac{h}{k} T_g}{\frac{h}{k} + \frac{R_0 \ln (R_0/R_1)}{(R_0/R_1)^2}} \quad (33)$$

The transient part of equation (26) is obtained by evaluating the summation for all roots of  $Z(p) = 0$  other than  $p = 0$ .

$$\frac{p dZ(p)}{dp} = \frac{p dE}{dp} \left[ \left( 1 + (R_0 - R_1) \left( \frac{B}{2} + \frac{h}{k} \right) \right) \cos [E(R_0 - R_1)] - E(R_0 - R_1) \sin [E(R_0 - R_1)] \right] \quad (34)$$

$$\frac{dE}{dp} = \frac{d \sqrt{-\left(\frac{B}{2}\right)^2 - \frac{p}{\alpha}}}{dp} = \frac{-\frac{1}{2\alpha}}{\sqrt{-\left(\frac{B}{2}\right)^2 - \frac{p}{\alpha}}} = \frac{-1}{2\alpha E} \quad (35)$$

$$\frac{Y(p) e^{pt}}{p \frac{dZ(p)}{dp}} = \frac{\frac{h}{k} T_g \sin [E(R_0 - R_1)] e^{pt}}{\frac{-p}{2\alpha E} \left[ \left( 1 + (R_0 - R_1) \left( \frac{B}{2} + \frac{h}{k} \right) \right) \cos [E(R_0 - R_1)] - E(R_0 - R_1) \sin [E(R_0 - R_1)] \right]} \quad (36)$$

Where the values of  $P$  have not yet been determined.

For  $Z(p) = 0$

$$0 = E \cos [E(R_0 - R_1)] + \left( \frac{B}{2} + \frac{h}{k} \right) \sin [E(R_0 - R_1)] \quad (37)$$

$$\text{or } \frac{E(R_0 - R_1)}{\left( \frac{B}{2} + \frac{h}{k} \right) (R_0 - R_1)} = -\tan [E(R_0 - R_1)] \quad (38)$$

which is the form

$$-\lambda_N = \tan \lambda \quad (39)$$

Where the infinite number of solutions satisfying this transcendental equation are the Eigenvalues. Equation (39) is easily solved graphically by simply plotting  $-\lambda_N$  and  $\tan \lambda$ . The points of intersection of the two expressions are then the Eigenvalues,  $\lambda_n$ . However, since

$$N = \frac{1}{\left(\frac{B}{2} + \frac{h}{k}\right) (R_o - R_i)} \quad (40)$$

it is therefore a function of the film coefficient,  $h$ , that we wish to solve for. It is first necessary then to assume a value of  $h$  in order to proceed. A logical first estimate for the film coefficient can be obtained by considering only the steady state portion of equation (26).

$$T_w = \frac{\frac{h}{k} T_g}{\frac{h}{k} + \frac{R_o \ln (R_o/R_i)}{(R_o - R_i)^2}} \quad (41)$$

$$\text{or } h_{\text{est}} = \left( \frac{K T_w}{T_g - T_w} \right) \frac{R_o \ln (R_o/R_i)}{(R_o - R_i)^2} \quad (42)$$

Using (42) in (40) it is then possible to draw the  $-N\lambda$  line and solve equation (39). It should be remembered that the calculated  $N$  value is applicable only at that point in the nozzle defined by  $B/2$  and at that value of  $K$  taken from the plot of integrated average thermal properties. Having found  $\lambda_n$  it is now possible to find  $P_n$  and  $E_n$ .

$$\lambda_n = (R_o - R_i) \sqrt{-\left(\frac{B}{2}\right)^2 - \frac{P}{\alpha}} \quad (43)$$

$$-\alpha \left[ \left( \frac{\lambda_n}{R_o - R_i} \right)^2 + \left( \frac{B}{2} \right)^2 \right] = P_n \quad (44)$$

$$E_n = \sqrt{-\left(\frac{B}{2}\right)^2 - \frac{(-\alpha) \left[ \left( \frac{\lambda_n}{R_o - R_i} \right)^2 + \left( \frac{B}{2} \right)^2 \right]}{\alpha}} = \frac{\lambda_n}{(R_o - R_i)} \quad (45)$$

(44), (45)  $\longrightarrow$  (36)

$$\frac{Y(p) e^{pt}}{P \frac{dZ(p)}{dp}} = \frac{\frac{h}{k} T_g \sin \lambda_n e^{-\alpha \left[ \left( \frac{\lambda_n}{R_o - R_i} \right)^2 + \left( \frac{B}{2} \right)^2 \right] t}}{\left[ \frac{\left( \frac{\lambda_n}{R_o - R_i} \right)^2 + \left( \frac{B}{2} \right)^2 \right] \left[ \left( 1 + (R_o - R_i) \left( \frac{B}{2} + \frac{h}{k} \right) \right) \cos \lambda_n - \lambda_n \sin \lambda_n \right]} \quad (46)$$

(33), (46) ————— (26)

$$T_w = \frac{h}{K} T_g \left[ \frac{1}{\frac{h}{k} + \frac{R_o \ln(R_o/R_i)}{(R_o - R_i)^2}} + \right. \\ \left. - \alpha \left[ \left( \frac{\lambda_n}{R_o - R_i} \right)^2 + \left( \frac{B}{2} \right)^2 \right] t \right] \\ \sum_{n=0}^{\infty} \frac{2 \lambda_n \sin \lambda_n e}{(R_o - R_i) \left[ \left( \frac{\lambda_n}{R_o - R_i} \right)^2 + \left( \frac{B}{2} \right)^2 \right]} \left[ \left( 1 + (R_o - R_i) \left( \frac{B}{2} + \frac{h}{k} \right) \right) \cos \lambda_n - \lambda_n \sin \lambda_n \right] \quad (47)$$

The solution of (47) for  $h$  will be biased because of the estimated film coefficient used to calculate  $N$ . It is then necessary to put the calculated value of  $h$  back into equation (40) and repeat the series of calculations. In this manner it is possible to iterate to find  $h$  to very close values.

Using the assembly drawings of the nozzle and the thermocouple temperature traces the following table is prepared prior to calculating the film coefficient.

Table I

Time Sec	R <sub>i</sub> Ft	R <sub>o</sub> Ft	T <sub>w</sub> -60°F °F	T <sub>g</sub> -520°R °F	K BTU Hr-Ft-°F	$\alpha$ Ft <sup>2</sup> /Hr
Thermocouple 11-2						
1	0.177	0.250	1520	5730	58.4	1.87
2	0.177	0.250	1920	5730	54.2	1.62
3	0.177	0.250	2120	5730	52.4	1.53
4	0.177	0.250	2370	5730	50.0	1.43
5	0.177	0.250	2460	5730	49.3	1.38
6	0.177	0.250	2680	5730	47.3	1.32
7	0.177	0.250	2830	5730	46.4	1.26
8	0.177	0.250	2920	5730	45.9	1.23
9	0.177	0.250	3010	5730	45.0	1.20
10	0.177	0.250	3060	5730	44.6	1.19
Thermocouple 11-3						
1	0.154	0.225	1940	5700	54.0	1.61
2	0.154	0.225	2140	5700	52.0	1.52
3	0.154	0.225	2390	5700	49.8	1.42
4	0.154	0.225	2560	5700	48.4	1.35
5	0.154	0.225	2610	5700	48.0	1.33
6	0.154	0.225	2680	5700	47.2	1.31
7	0.154	0.225	2700	5700	47.1	1.31
8	0.154	0.225	2700	5700	47.1	1.31
9	0.154	0.225	2710	5700	47.0	1.30
10	0.154	0.225	2730	5700	47.0	1.29
Thermocouple 11-4						
1	0.167	0.240	1900	5240	54.3	1.64
2	0.167	0.240	2270	5240	50.4	1.47
3	0.167	0.240	2640	5240	47.7	1.32
4	0.167	0.240	2880	5240	45.4	1.25
5	0.167	0.240	2960	5240	45.2	1.22
6	0.167	0.240	2960	5240	45.2	1.22
7	0.167	0.240	3000	5240	45.0	1.20
8	0.167	0.240	3080	5240	44.4	1.19
9	0.167	0.240	3090	5240	44.3	1.18
10	0.167	0.240	3100	5240	44.2	1.18

Table I (cont'd)

Time Sec	R <sub>i</sub> Ft	R <sub>o</sub> Ft	T <sub>w</sub> -60°F °F	T <sub>g</sub> -520°R °F	K BTU Hr-Ft-°F	α Ft <sup>2</sup> /Hr
Thermocouple 11-8						
1	0.167	0.240	1440	5240	59.0	1.92
2	0.167	0.240	1860	5240	54.7	1.67
3	0.167	0.240	2100	5240	52.3	1.55
4	0.167	0.240	2380	5240	49.8	1.43
5	0.167	0.240	2480	5240	49.2	1.38
6	0.167	0.240	2580	5240	48.2	1.34
7	0.167	0.240	2700	5240	47.1	1.31
8	0.167	0.240	2740	5240	46.9	1.29
9	0.167	0.240	2760	5240	46.7	1.28
10	0.167	0.240	2770	5240	46.6	1.28
Thermocouple 51						
1	0.208	0.275	1780	5750	55.2	1.72
2	0.208	0.275	2040	5750	52.8	1.57
3	0.208	0.275	2090	5750	52.4	1.55
4	0.208	0.275	2190	5750	51.5	1.50
5	0.208	0.275	2310	5750	50.3	1.45
6	0.208	0.275	2530	5750	48.6	1.37
7	0.208	0.275	2780	5750	46.5	1.28
8	0.208	0.275	2890	5750	45.9	1.24
9	0.208	0.275	2810	5750	46.4	1.27
10	0.208	0.275	2640	5750	47.7	1.29
Thermocouple 52						
1	0.177	0.250	2340	5730	50.2	1.43
2	0.177	0.250	2760	5730	46.7	1.28
3	0.177	0.250	2600	5730	48.0	1.33
4	0.177	0.250	2590	5730	48.0	1.34
5	0.177	0.250	2600	5730	48.0	1.33
6	0.177	0.250	2710	5730	47.0	1.31
7	0.177	0.250	2540	5730	48.5	1.37
8	0.177	0.250	2140	5730	52.0	1.52
9	0.177	0.250	1510	5730	58.4	1.88
10	0.177	0.250	1510	5730	58.4	1.88

Table I (cont'd)

Time Sec	R <sub>i</sub> Ft	R <sub>o</sub> Ft	T <sub>w</sub> -60°F °F	T <sub>g</sub> -520°R °F	K BTU Hr-Ft-°F	$\alpha$ Ft <sup>2</sup> /Hr
Thermocouple 54						
1	0.167	0.240	1890	5240	54.3	1.65
2	0.167	0.240	2160	5240	52.0	1.52
3	0.167	0.240	2160	5240	52.0	1.52
4	0.167	0.240	2220	5240	51.2	1.48
5	0.167	0.240	2290	5240	50.5	1.46
6	0.167	0.240	2450	5240	49.3	1.39
7	0.167	0.240	2520	5240	48.6	1.37
8	0.167	0.240	2540	5240	48.5	1.37
9	0.167	0.240	2520	5240	48.6	1.37
10	0.167	0.240	2540	5240	48.5	1.37
Thermocouple 57						
1	0.167	0.240	2480	5240	49.0	1.33
2	0.167	0.240	2880	5240	46.0	1.24
3	0.167	0.240	2740	5240	46.9	1.29
4	0.167	0.240	2740	5240	46.9	1.29
5	0.167	0.240	2740	5240	46.9	1.29
6	0.167	0.240	3040	5240	44.6	1.19
7	0.167	0.240	3170	5240	43.8	1.16
8	0.167	0.240	2990	5240	45.0	1.20
9	0.167	0.240	2810	5240	46.4	1.27
10	0.167	0.240	2710	5240	47.0	1.31

Table II

Time	R <sub>i</sub>	R <sub>o</sub>	T <sub>w</sub> -60°F °F	T <sub>g</sub> -520°R °F	K BTU Hr-Ft-°F	$\alpha$ Ft <sup>2</sup> /Hr
Thermocouple 11-5						
10	0.225	0.283	3120	4805	0.266	0.003
Thermocouple 11-6						
10	0.317	0.367	2730	4250	0.266	0.003



A Fortran listing of the computer program is given below.

```
104  FORMAT (45HEXPERIMENTAL HT TRANSFER COEFF-INPUT THEN ANS/)
      PUNCH 104
100  FORMAT (7F10.3)
101  FORMAT (21H HT TRANSFER COEFF = ,F10.1)
200  READ100,TW,TG,RO,RI,TK,TT,ALPH
      PUNCH100,TW,TG,RO,RI,TK,TT,ALPH
      T=TT/3600.
      B=(LOG(RO/RI))/(RO-RI)
      AH=TK*(B*RO/(RO-RI))*TW/(TG-TW)
80   R=1./((B/2.+AH/TK)*(RO-RI))
      SGMA=1./(AH/TK+B*RO/(RO-RI))
      P=0.
25   GAM1=(P+.5)*3.1415927+.001
20   TANG=SIN(GAM1)/COS(GAM1)
      GAM2=GAM1-(TANG+R*GAM1)/(R+1.-R*GAM1*TANG)
      IF(ABSF(GAM2-GAM1)-.0001)30,10,10
10   GAM1=GAM2
      GO TO 20
30   E =ALPH*((GAM2/(RO-RI))**2+(B/2. )**2)*T
      Z=GAM2*(SIN(GAM2))*(2.7183**(-E))
      D=((GAM2/(RO-RI))**2+(B/2. )**2)*(RO-RI/(2.*Z)
      C3=D*((COS(GAM2)*(1.+(RO-RI)*(B/2. )))-GAM2*SIN(GAM2))
      C4=D*((RO-RI)*COS(GAM2))
      X=1./(C3+C4*AH/TK)
      SGMA=SGMA+X
      IF(ABSF(X)-.001)50,40,40
```

```
40 P=P+1.  
    GO TO 25  
50 BH=AH  
    AH=TK*(TW/TG)/SGMA  
    IF (ABSF(AH-BH) - .1) 70,70,80  
70 PUNCH 101,AH  
    GO TO 200  
END
```

Calculated values of the film coefficient are given in Table III for the first ten seconds of the tests. See Figure 34.

Table III

Thermo- couple	Film Coefficient - BTU/Hr-Ft <sup>2</sup> -°F									
	1 sec	2 sec	3 sec	4 sec	5 sec	6 sec	7 sec	8 sec	9 sec	10 sec
11-2	808.7	794.6	783.6	781.6	761.2	805.3	843.4	859.7	875.6	880.5
11-3	1130.6	934.2	912.5	899.3	852.3	830.8	804.6	779.8	766.8	765.2
11-4	1229.5	1142.5	1226.6	1249.9	1218.0	1142.6	1123.0	1137.7	1116.8	1101.6
11-5	--	--	--	--	--	--	--	--	--	11.5
11-6	--	--	--	--	--	--	--	--	--	10.0
11-8	847.0	861.8	852.5	912.3	901.5	901.1	923.6	919.4	908.0	896.4
51	970.1	845.9	730.2	695.0	690.1	744.8	822.6	854.0	798.1	719.1
52	1446.7	1346.3	1018.7	891.1	824.1	818.1	710.8	545.9	352.8	348.5
54	1216.6	1072.0	893.4	824.4	791.3	830.1	827.2	811.3	782.8	779.5
57	1833.8	1731.0	1306.6	1155.0	1058.8	1204.4	1250.9	1076.7	937.2	862.0

A complete set of values was not obtained for thermocouples 11-5 and 11-6 because the first series of calculations at 10 seconds were observed to be two orders of magnitude away from most of the other points. This was expected, however since the mathematical model being used in this analysis makes no attempt to include the effects of ablation. The entire nozzle wall and indeed the phenolic thermocouples themselves are eroded away in the exit cone apparently voiding any analysis that does not include an ablative boundary. Calculations were not performed on any of the other phenolic thermocouples for the same reason.

As stated in the objectives, it was desired to compare the values of film coefficients as calculated from the proposed technique with those given by other investigations based on boundary layer concepts and convection only. A recent investigation of this type is one performed by High Temperature Materials, Inc. of Boston Massachusetts<sup>3</sup>. Their results are arrived at through the use of the popular Bartz equation<sup>4</sup>.

$$h = \left[ \frac{0.026}{D_*^{0.2}} \left( \frac{\mu^{0.2} C_p}{P_r^{0.6}} \right)_0 \left( \frac{P_c}{C^*} \right)^{0.8} \left( \frac{D_*}{r_c} \right)^{0.1} \right] \left( \frac{A_*}{A} \right)^{0.9} \sigma \quad (48)$$

where

$$\sigma = \frac{1}{\left[ \frac{1}{2} \frac{T_w}{T_0} \left( 1 + \left( \frac{\gamma-1}{2} \right) M^2 \right) + \frac{1}{2} \right]^{0.8} \left( \frac{\gamma}{5} \right) \left[ 1 + \left( \frac{\gamma-1}{2} \right) M^2 \right]^{1/5}} \quad (49)$$

Film coefficient values from Table III are compared with those predicted by High Temperature Materials, Inc. (HTM) in Figure 35. It should be noted that the predictions of HTM are based on the exact same nozzle as the current study. Both studies used theoretical gas temperatures as predicted by a Hercules Powder Company computer program entitled, "Free Energy Calculation No. 0148."

The main point of deviation between the two studies as far as input information is concerned is in the wall temperatures used. High Temperature Materials, Inc. used wall temperatures based on an assumed recovery factor of 0.815 which would place the temperature of the wall considerably higher than free stream temperature. The recorded temperatures used in the present analysis are seen to be nearly half of free stream temperature. This discrepancy is to be expected, however since the physical model assumed by HTM did not account for the fact that the nozzle wall is a very good heat sink.

The major point of deviation in the final results is in the transient behavior of the present study. This is evident from the first five seconds of Figure 25 but is more graphically exhibited in Figure 26 when compared with the HTM data. Film coefficient curves are seen to reduce in magnitude and shift downstream slightly with successive time increments. Unfortunately, it was not possible to place a thermocouple in the throat area. A few readings

in the throat area would enable one to sketch in a continuous curve for the entire nozzle length rather than only having an indication in the approach and a single point in the exit cone. Two other general observations can be made from Figure 26 in that the film coefficient values presented here form the skeleton of a curve or family of curves that have a broader peak and are also higher in magnitude than the HTM data based on convection. The importance of radiation and other non-convective heat transfer factors can be observed in the nozzle approach section because of the very high film coefficient values compared with those based on convection only. This would be expected, however since there is a larger deviation between gas and wall temperatures in the approach than in later parts of the nozzle. This would give increased importance to the fourth power radiational heating.

Considerable scattering of the data is present owing to the jagged temperature curves. Continued testing and experience with the type of thermocouples used in this study should reduce the scatter and produce more definitive curves of the overall film coefficient. Less scatter is observed within an individual test than between tests.

## CONCLUSIONS AND RECOMMENDATIONS

Many conclusions concerning the heat flux in solid fuel rocket nozzles can be drawn from this experiment. Some of them will have to await further experimentation for verification or correction while others are self-evident. Some of the more important conclusions are:

1. Film coefficients and therefore heat fluxes are much higher in value in the nozzle approach section than they have been considered to be in the past. This anomaly is apparently due to the lack of prior studies to include radiational effects.

2. The curve showing film coefficient versus nozzle position (Figure 26) shows the transient effect of time in that the calculated values decrease in magnitude with each successive time increment. The curves given by this analysis are also seen to extend farther into the nozzle approach region and to have a broader peak than the curve predicted by convection only.

3. Assuming that the High Temperature Materials, Inc. data based on the Bartz equation is representative of film coefficients for convective heat transfer only; then the convective heat transfer method is seen to be inadequate for design purposes in the approach section of the nozzle for short duration firings. It would be very difficult on the strength of such a small amount of data to establish a relationship between convective and total heat transfer. It can be said however, that to apply a constant multiplying factor to the convective film coefficient could result in a heavily overdesigned nozzle in some areas.

4. It can be concluded that the mathematical model presented in this paper is inadequate to describe film coefficients where the wall is composed of an ablative material.

On the basis of the single experiment performed in this study there are a number of recommendations that can be made for further work.

1. It is recommended that additional experiments be carried out to refine the data presented in this study.

2. Several changes are suggested in the thermocouples to be used on later tests. Thermocouples in the exit cone should probably be platinum/platinum-rhodium to prevent the sensing tip from protruding into the gas boundary layer. The tapered center core of the thermocouples should either be potted or locked in to prevent its loss. An attempt should be made to place a thermocouple nearer the throat of the nozzle.

3. The mathematical model should be extended to cover nozzle walls composed of several layers of dissimilar materials. It should also be extended to include the effects of ablation.

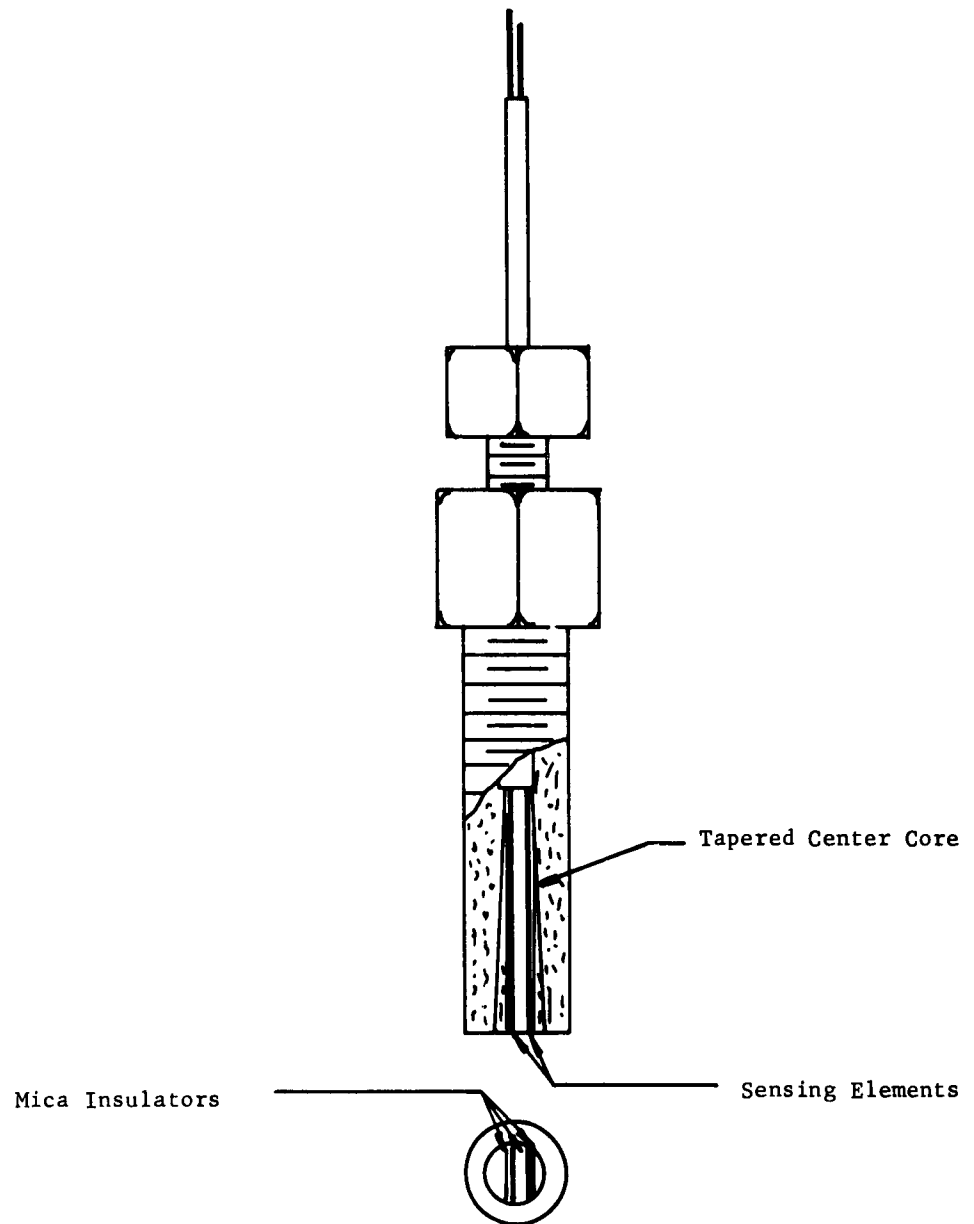


Figure 1 Namac Model "P" Thermocouple



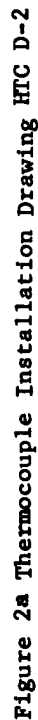








Figure 3 First Test Motor with Nozzle Prior to Firing



Figure 4 Second Test Motor With Nozzle Prior to Firing

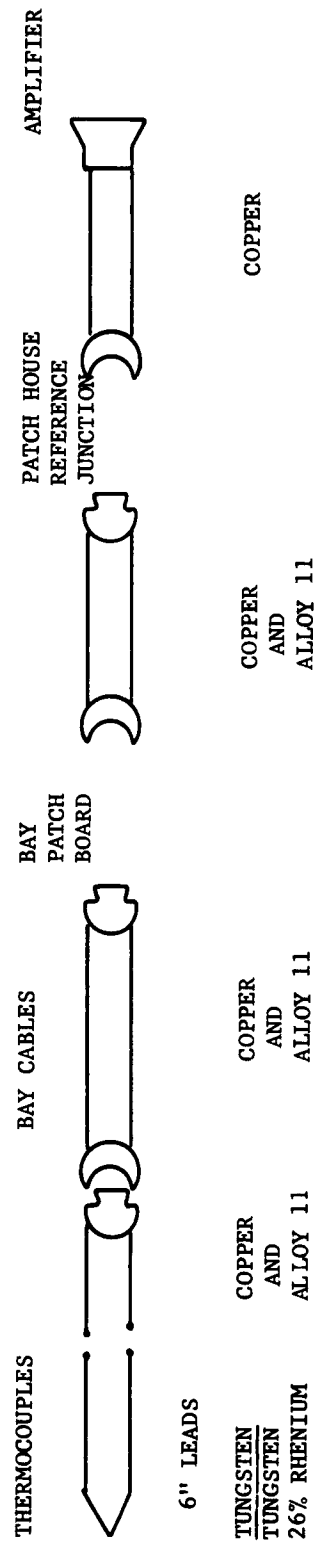


Figure 5 Thermocouple to Instrument House Circuit



Figure 6 HTC D-2 After Firing



Figure 7 HTC D-2 After Firing



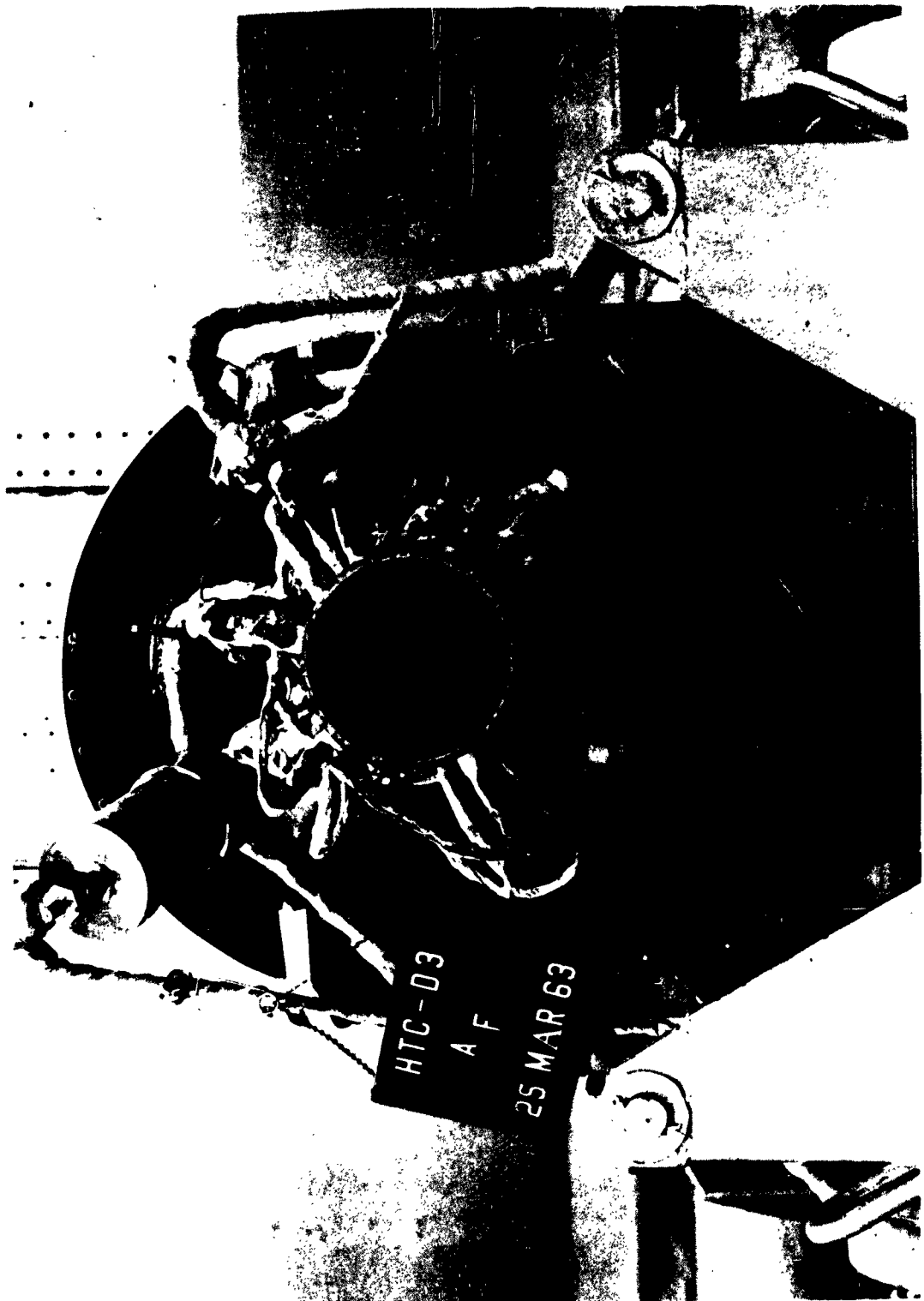


Figure 8 HTC D-3 After Firing

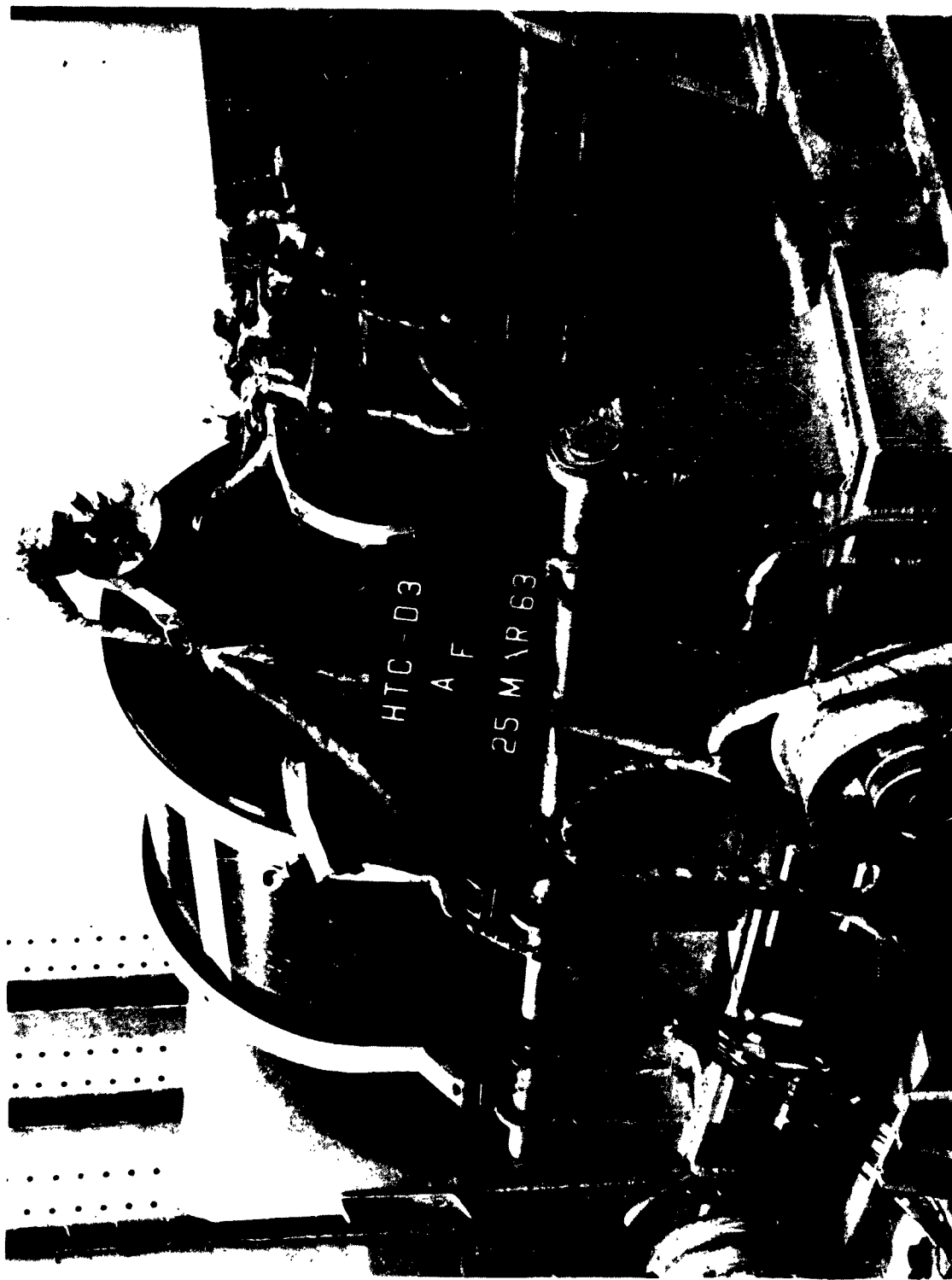


Figure 9 HTC D-3 After Firing

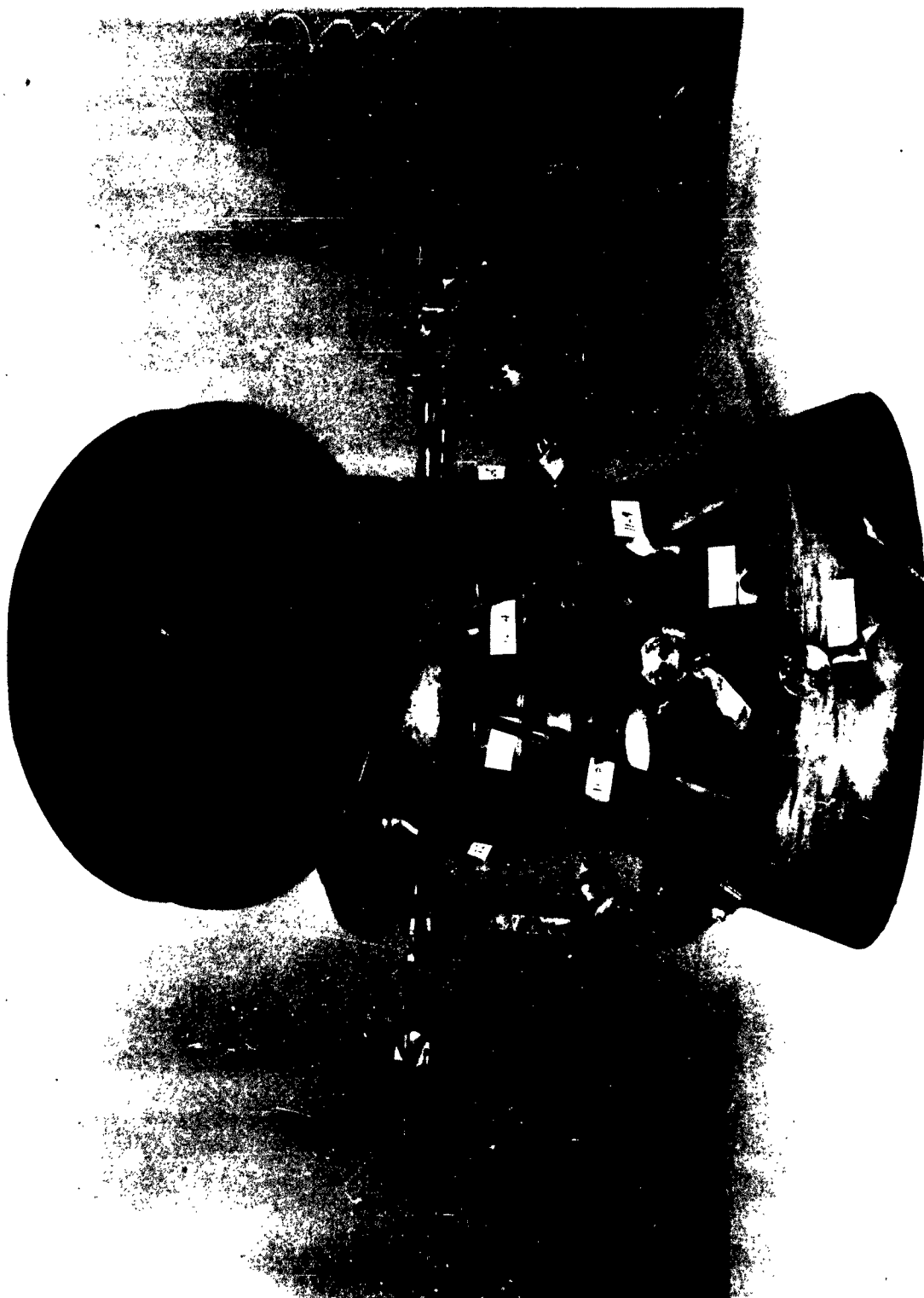


Figure 10 Instrumented Nozzle After Firing



Figure 11 Instrumented Nozzle After Firing



Figure 11 Instrumented Nozzle After Firing

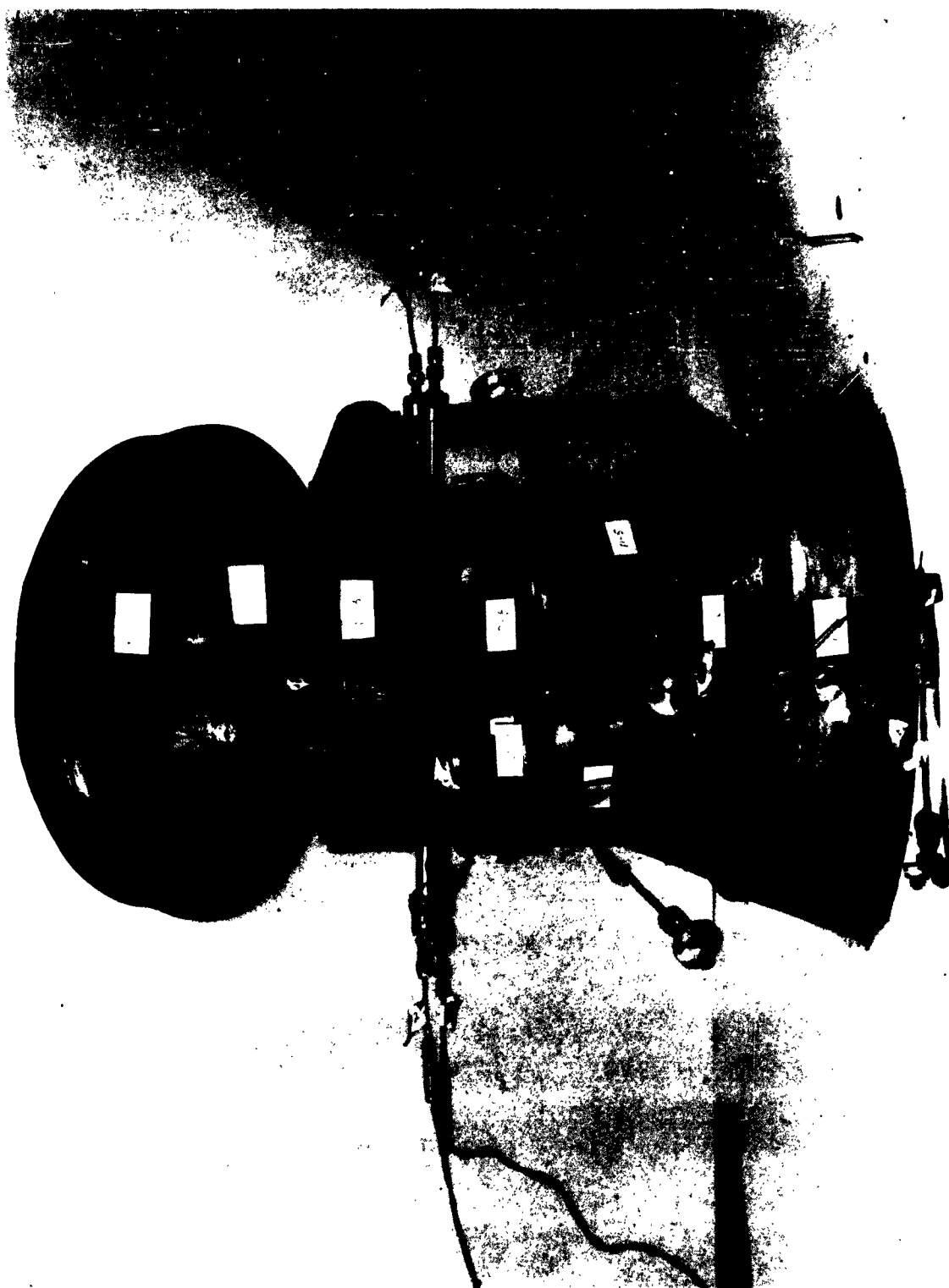


Figure 12 Instrumented Nozzle After Firing

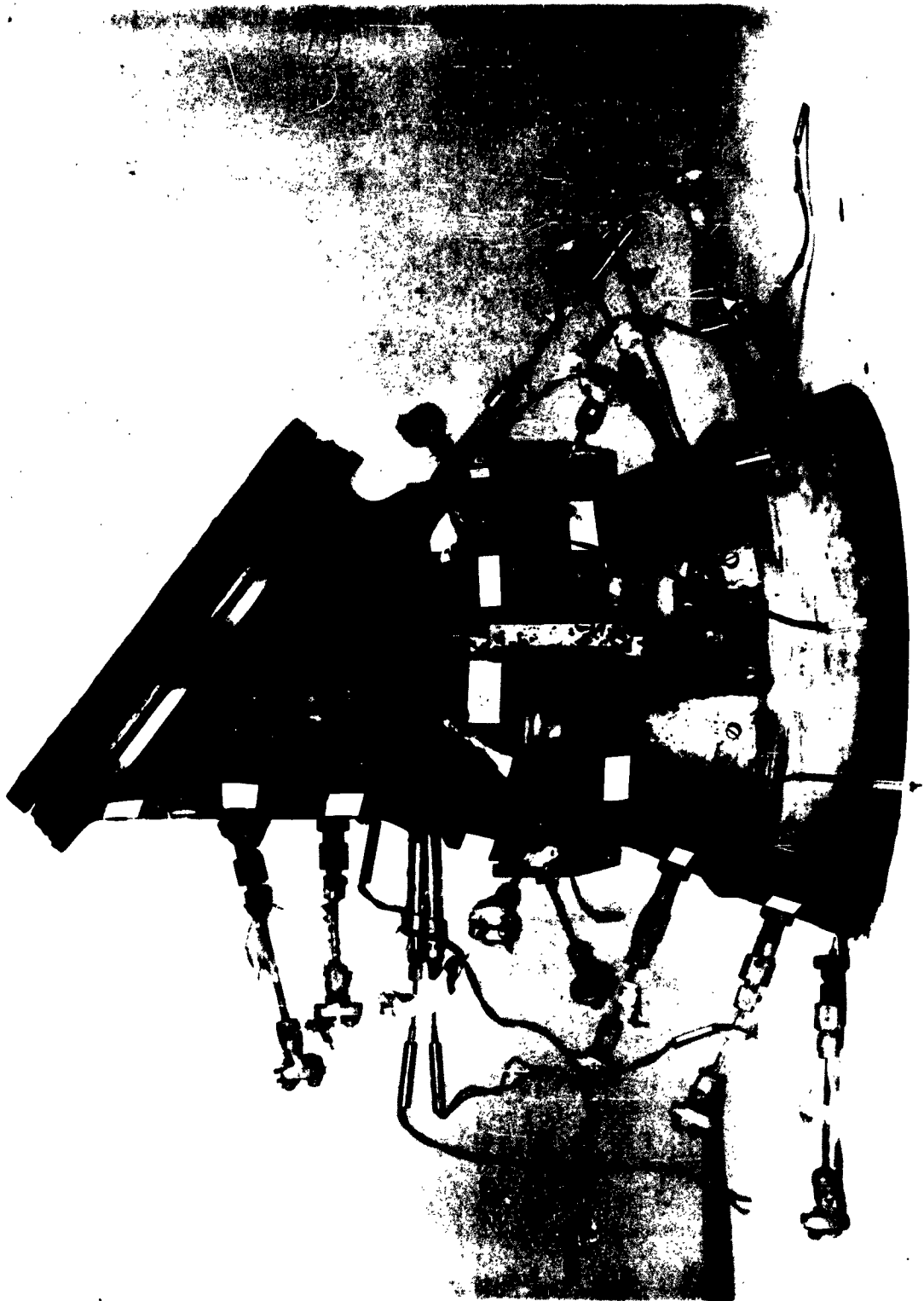


Figure 13 Instrumented Nozzle After Firing



Figure 14 Instrumented Nozzle After Firing



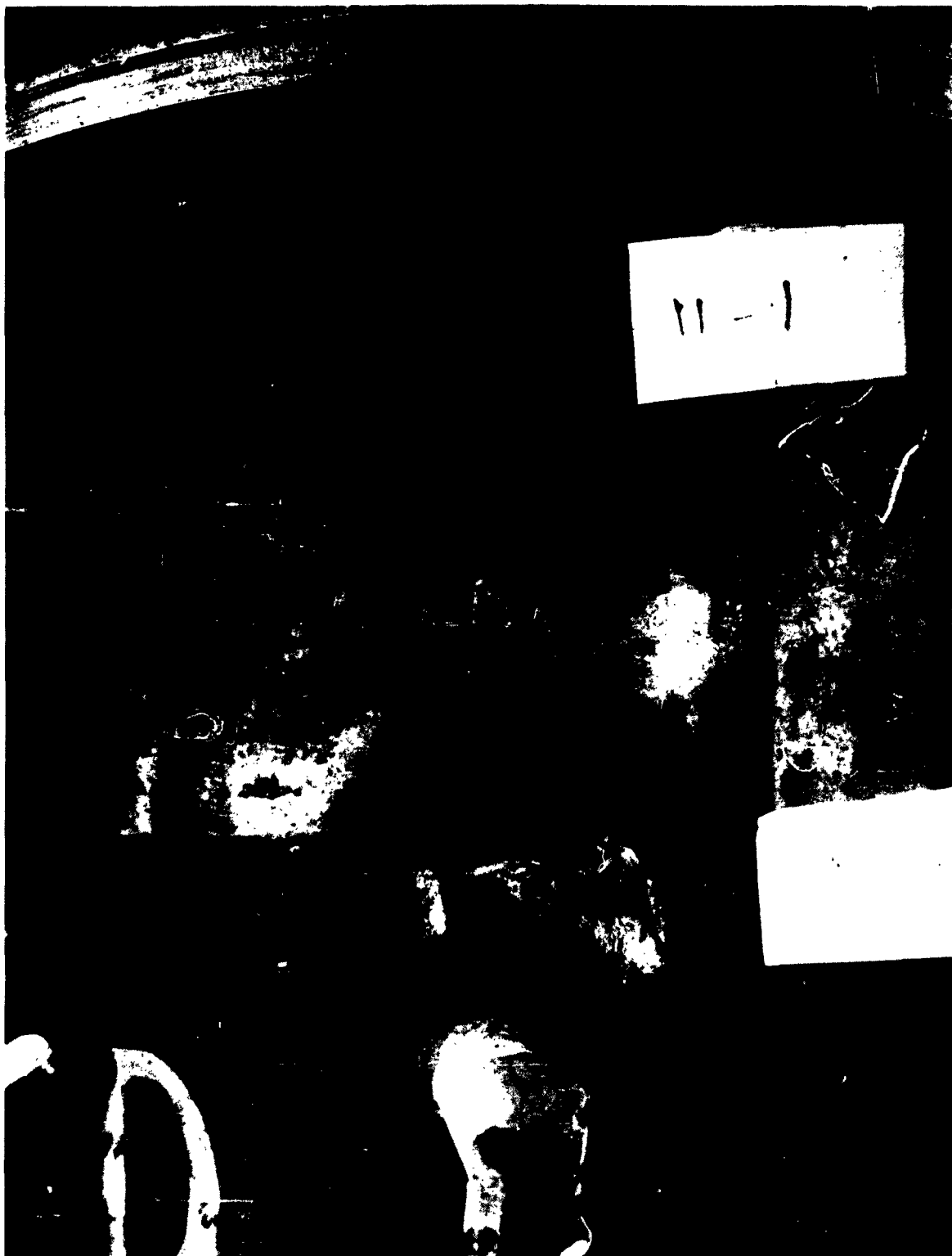


Figure 15 Broken Thermocouples

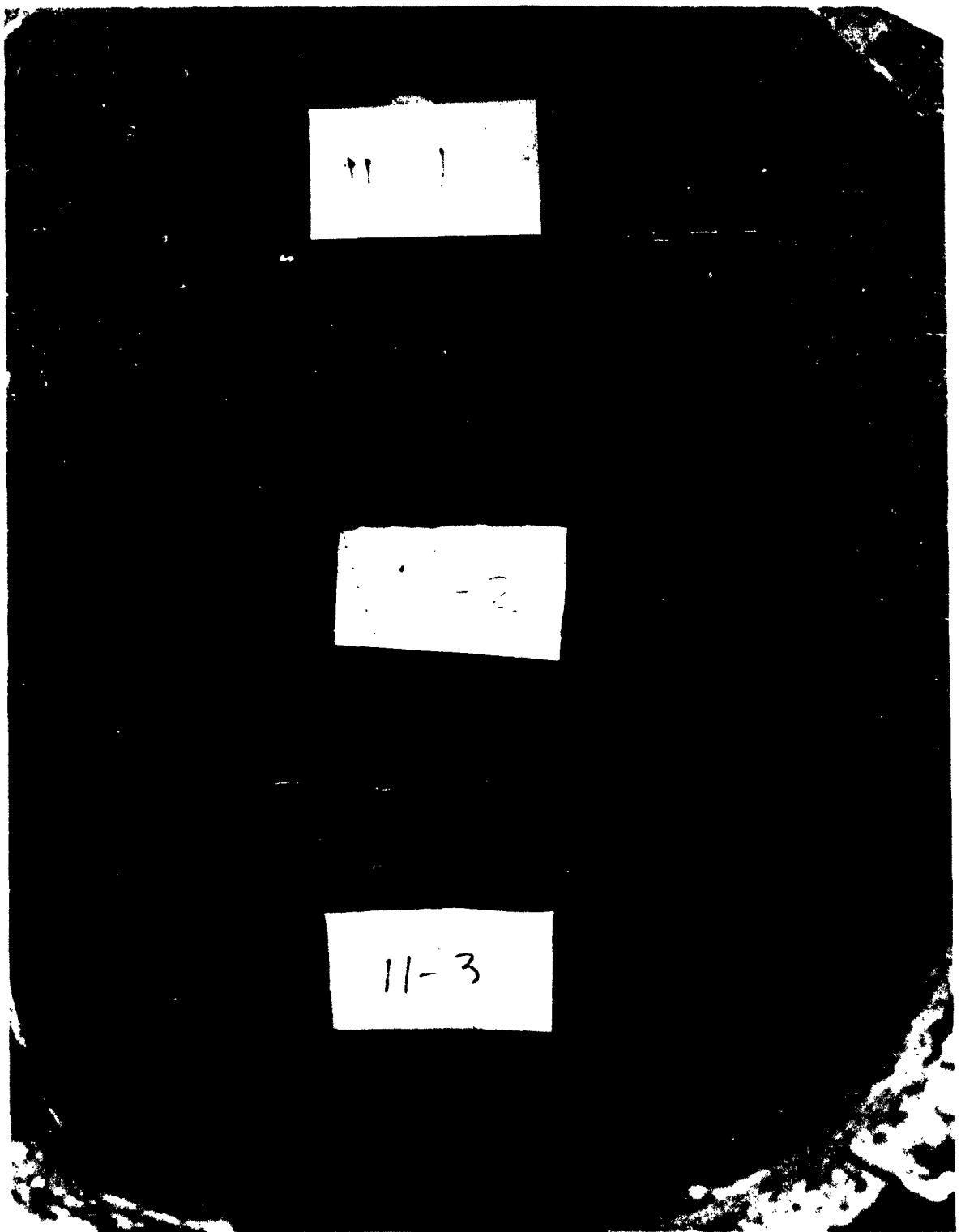


Figure 16 Thermocouple 11-2 Showing Loss of Inside Core

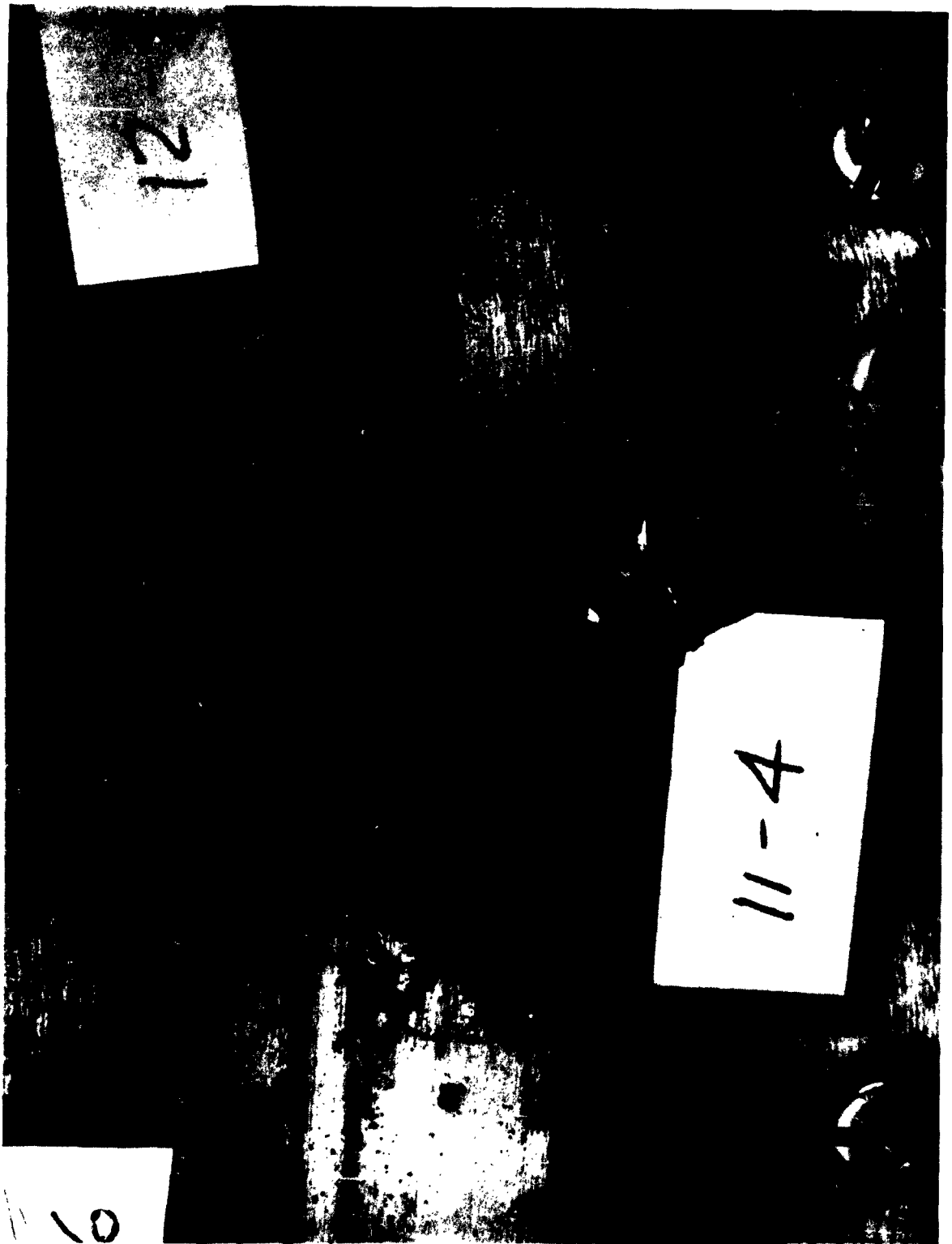


Figure 17 Gas Leak Around TC 11-4



Figure 18 Gas Leak Around TC 11-8

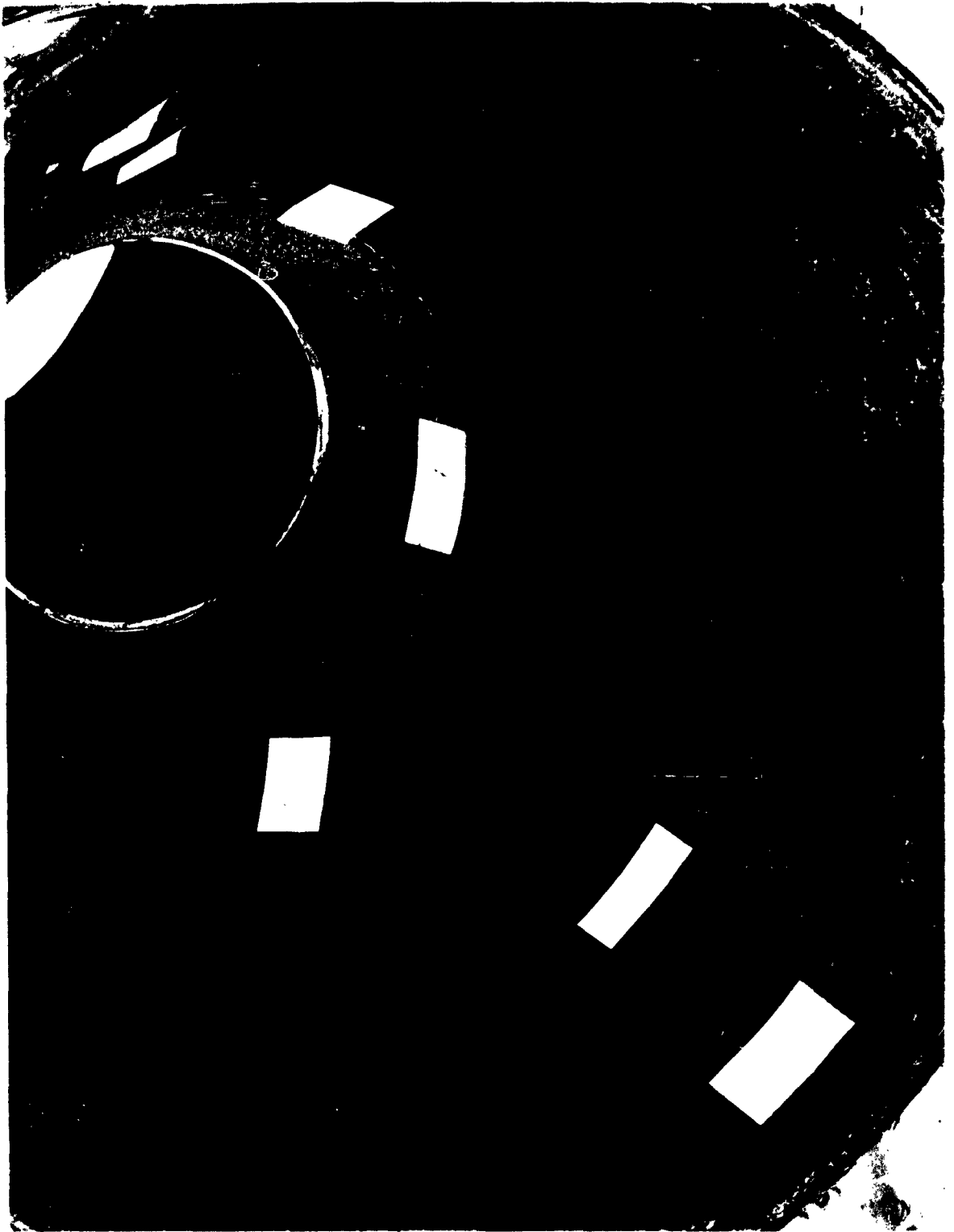


Figure 19 Erosion Around TC 11-4

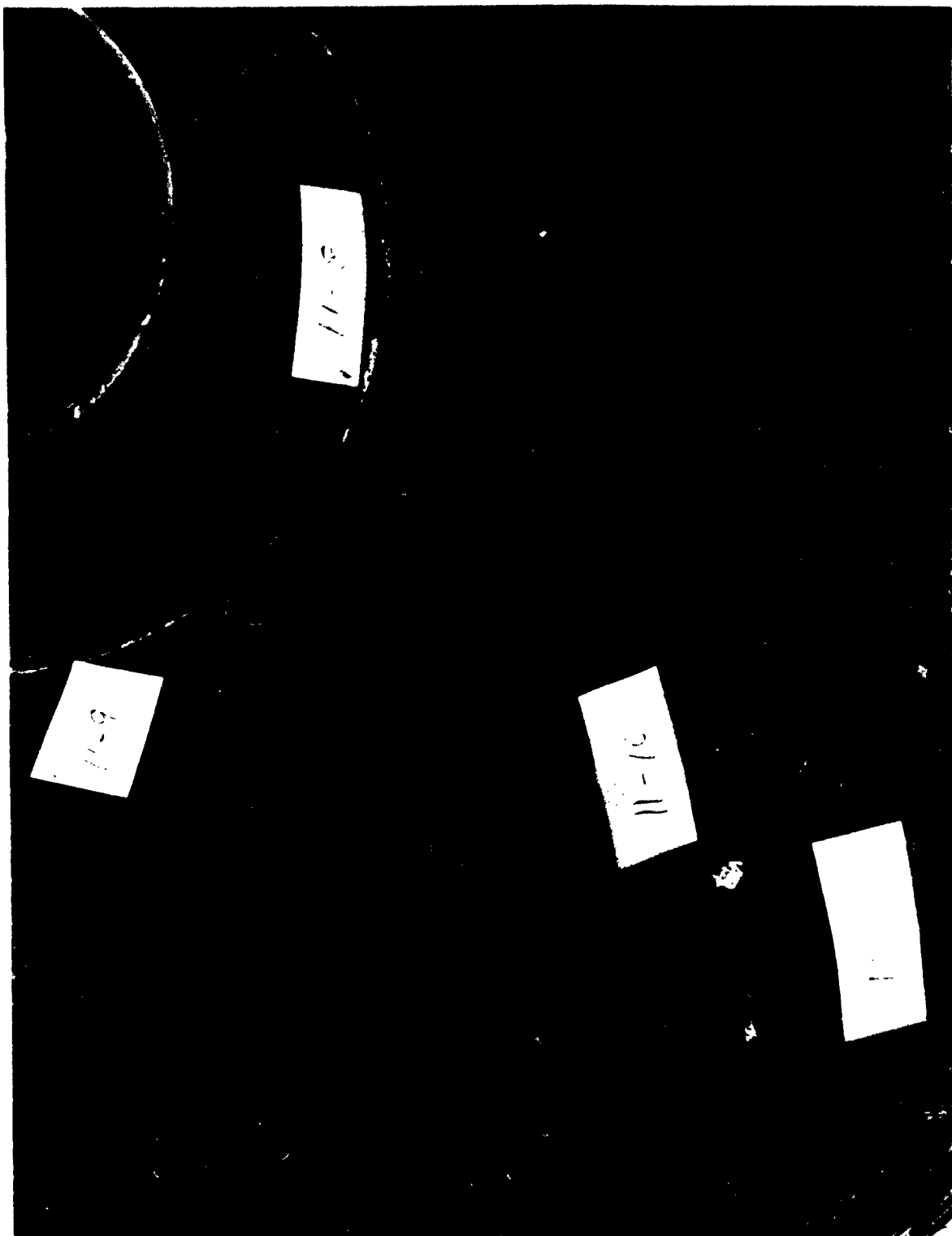
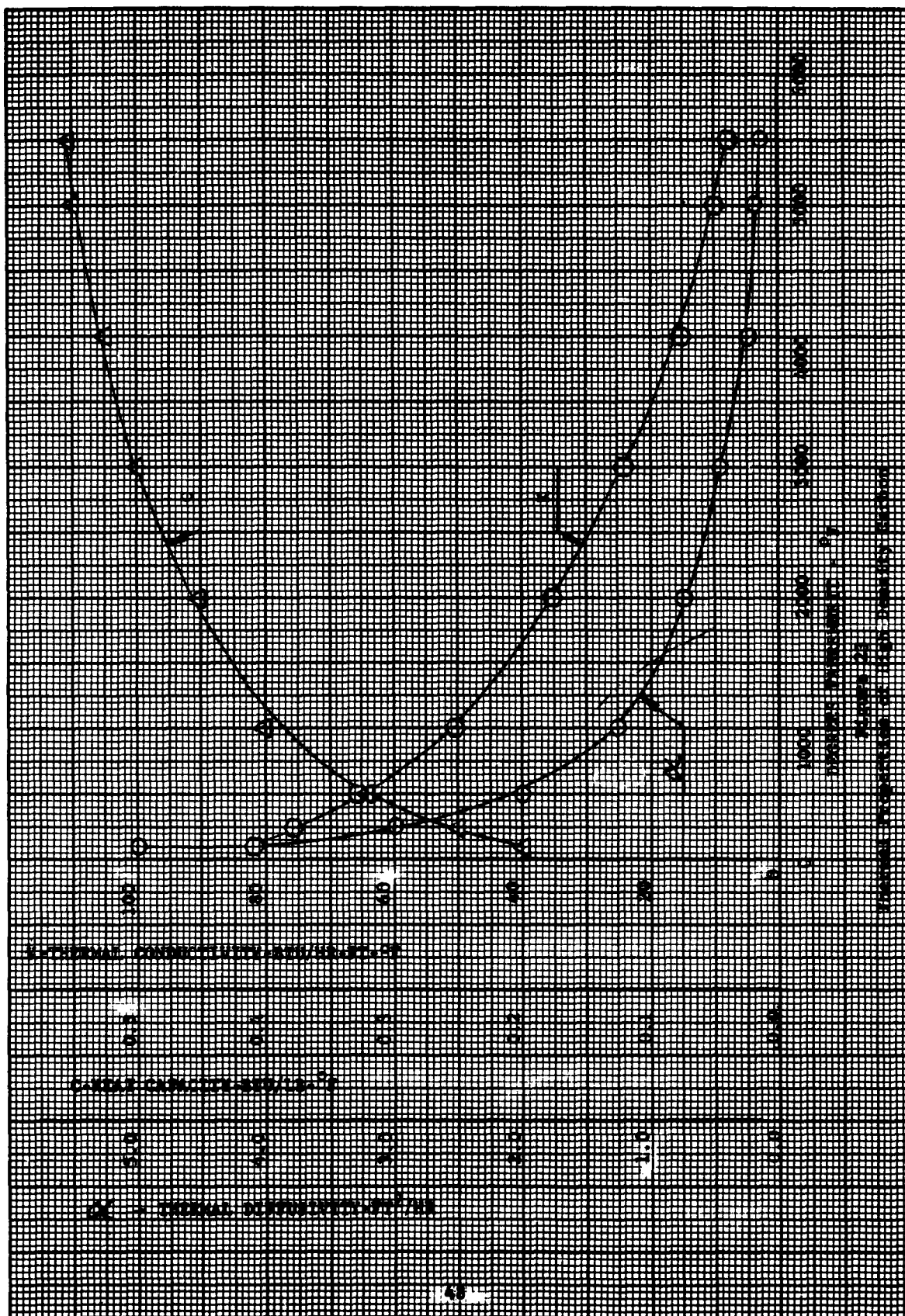
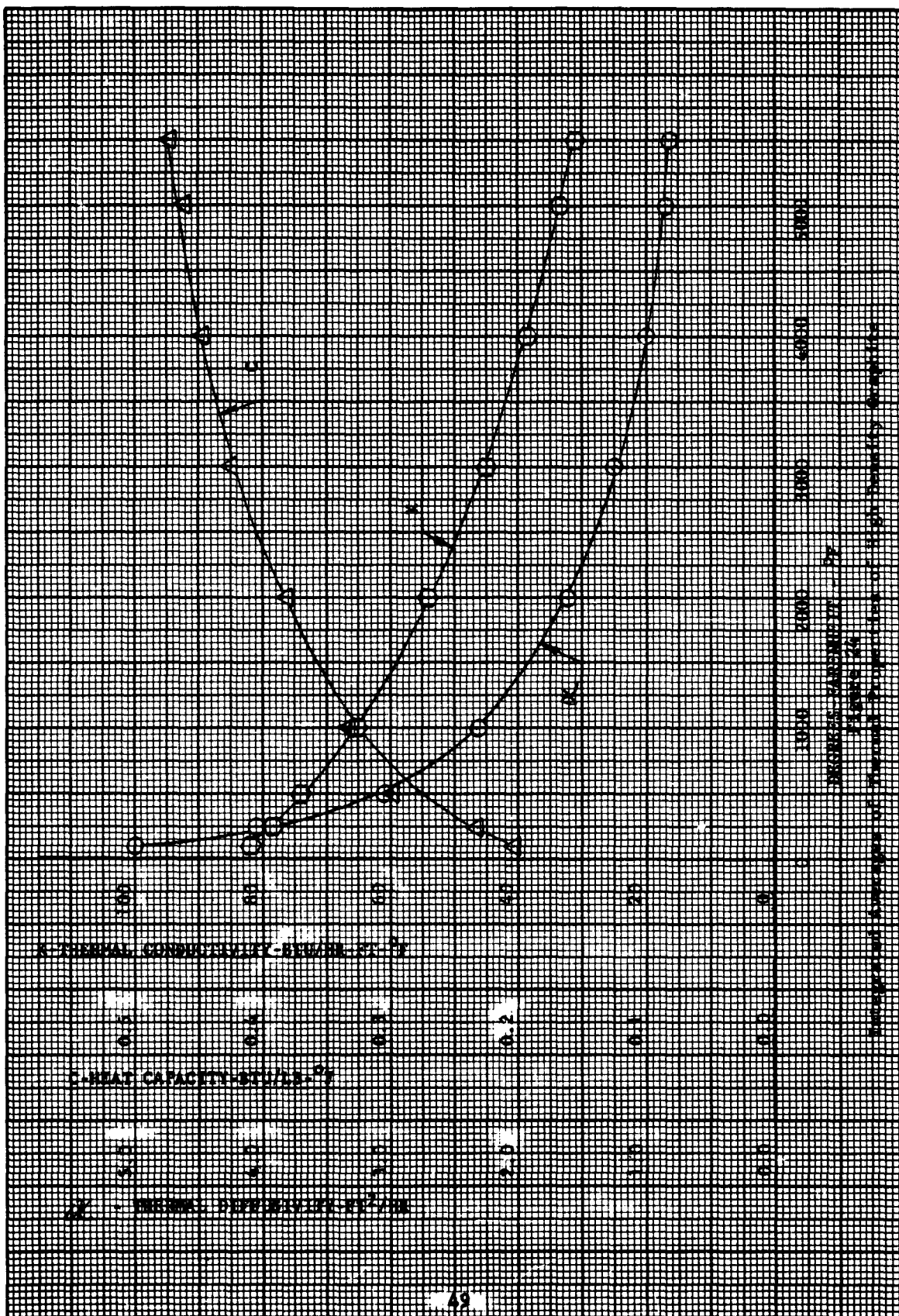
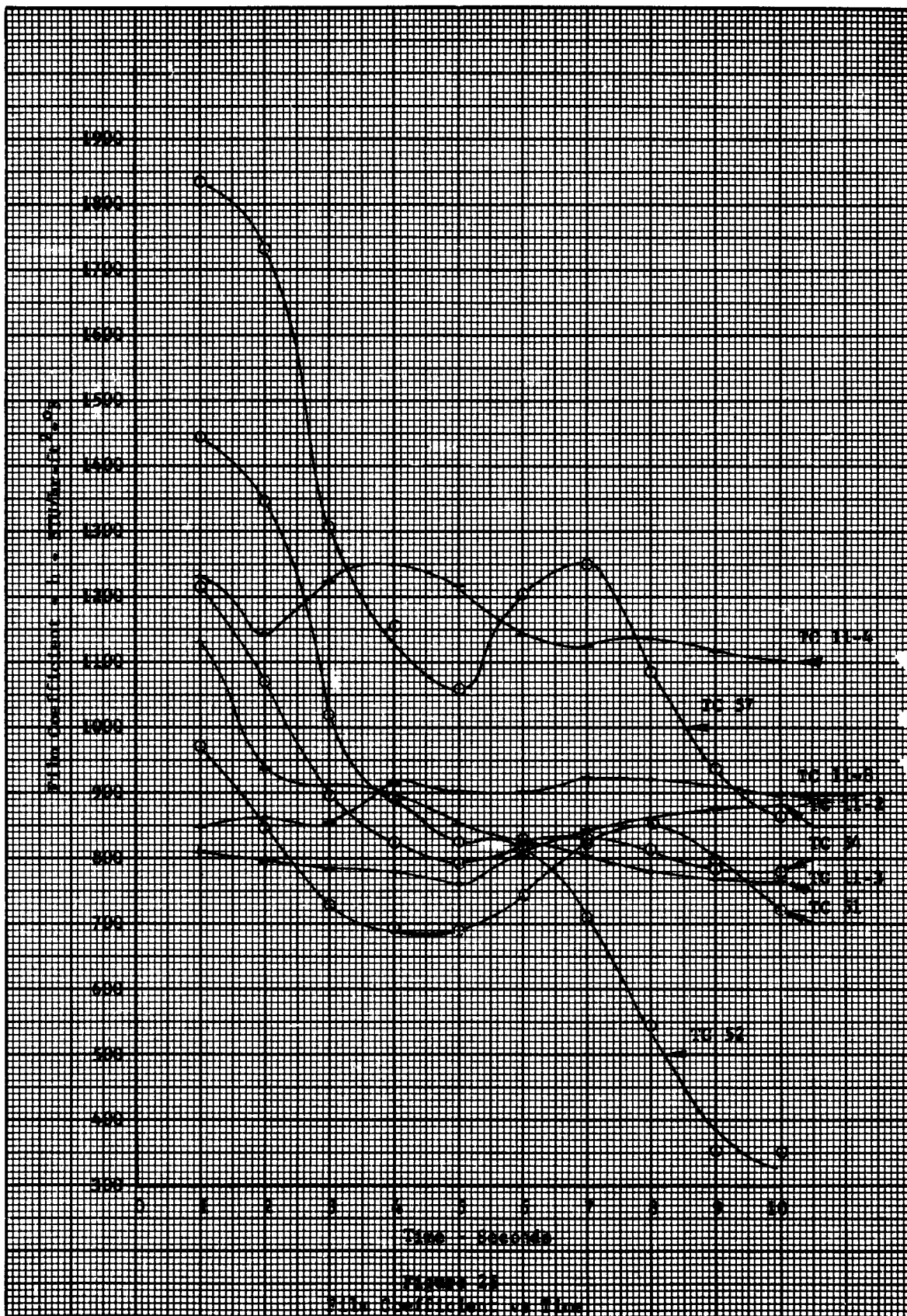


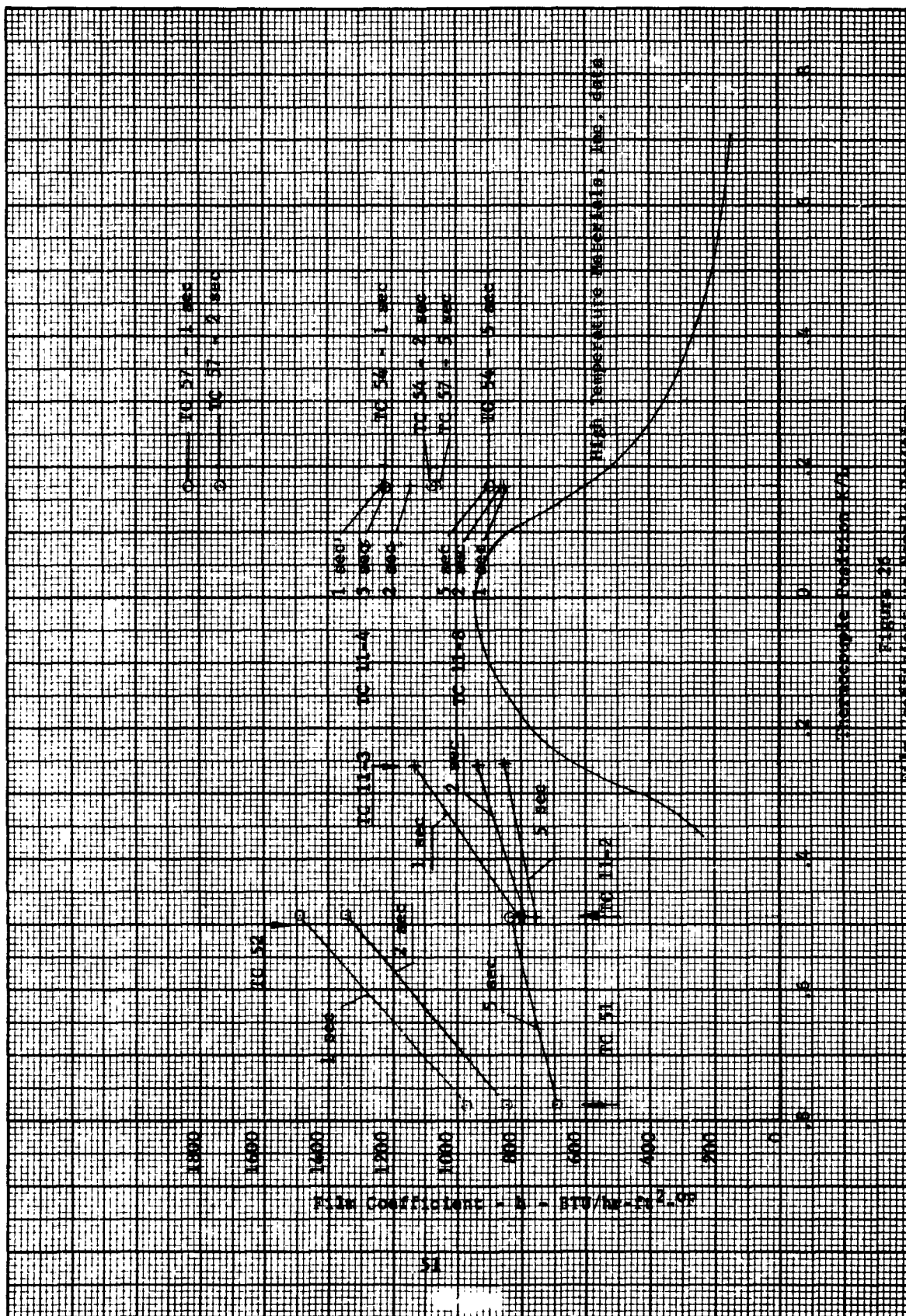
Figure 20 Erosion Around TC 11-8











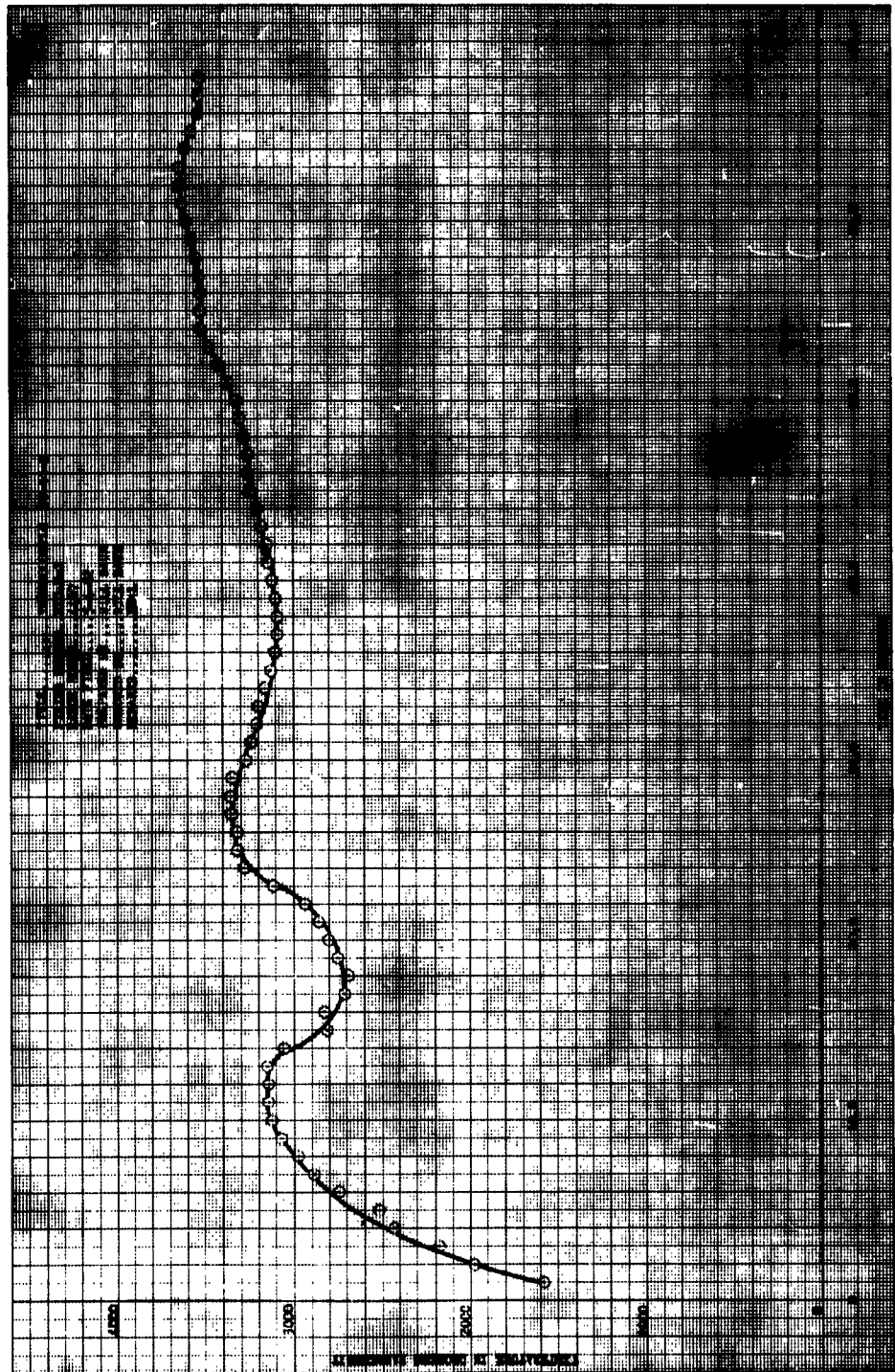


Figure 27 Temperature Plot, TC 11-2

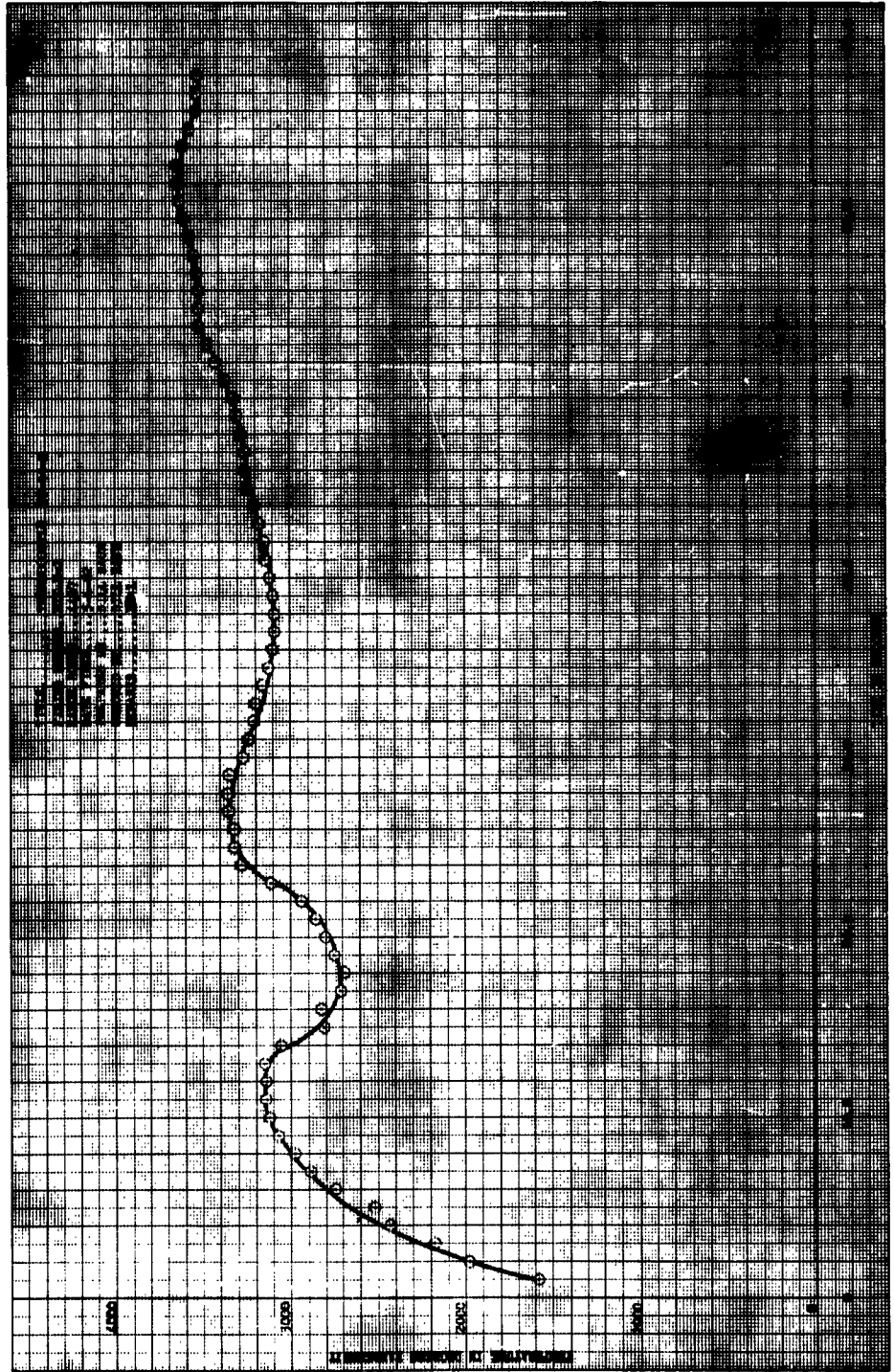


Figure 27 Temperature Plot, TC 11-2

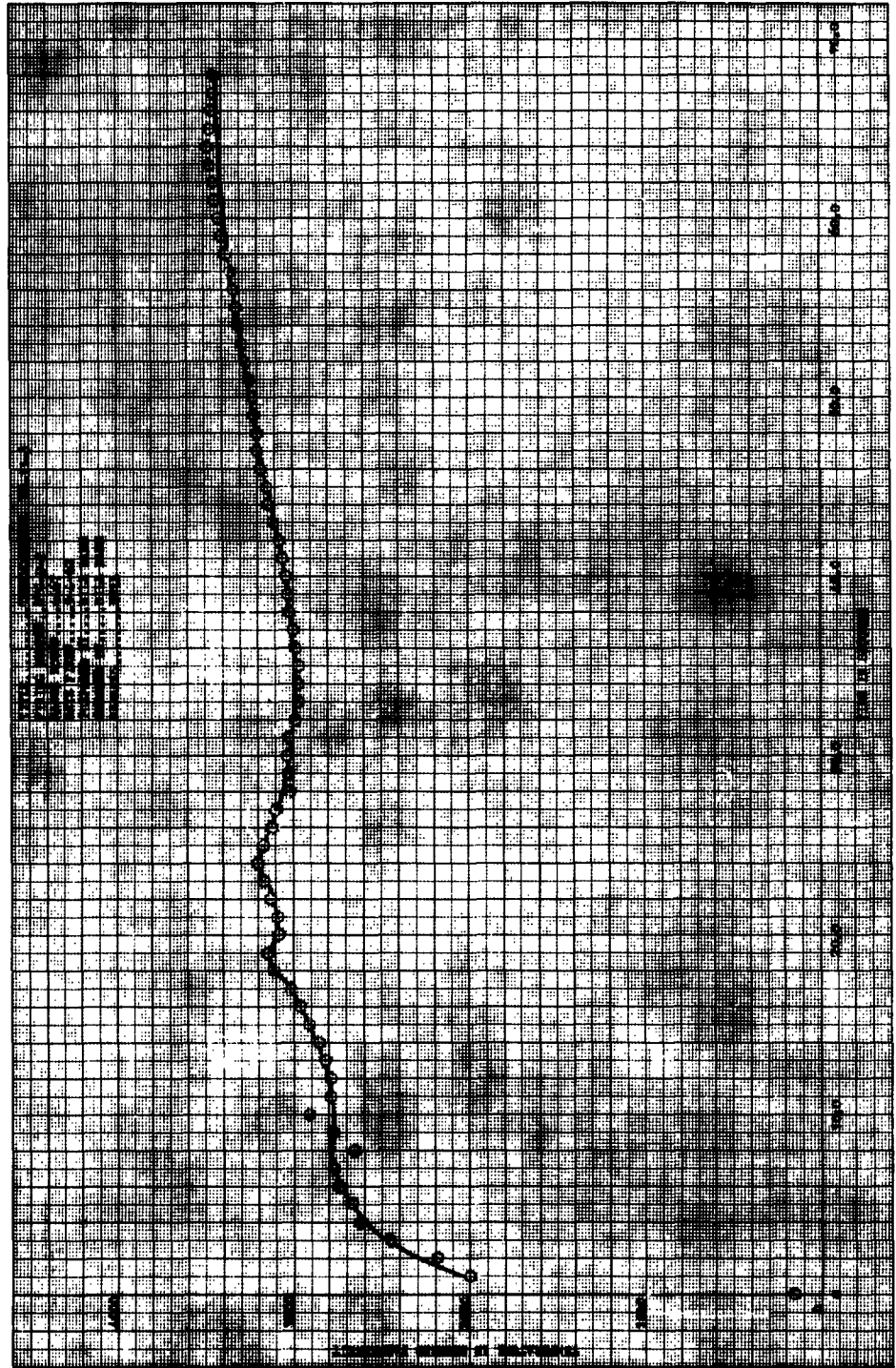


Figure 28 Temperature Plot, TC 11-3



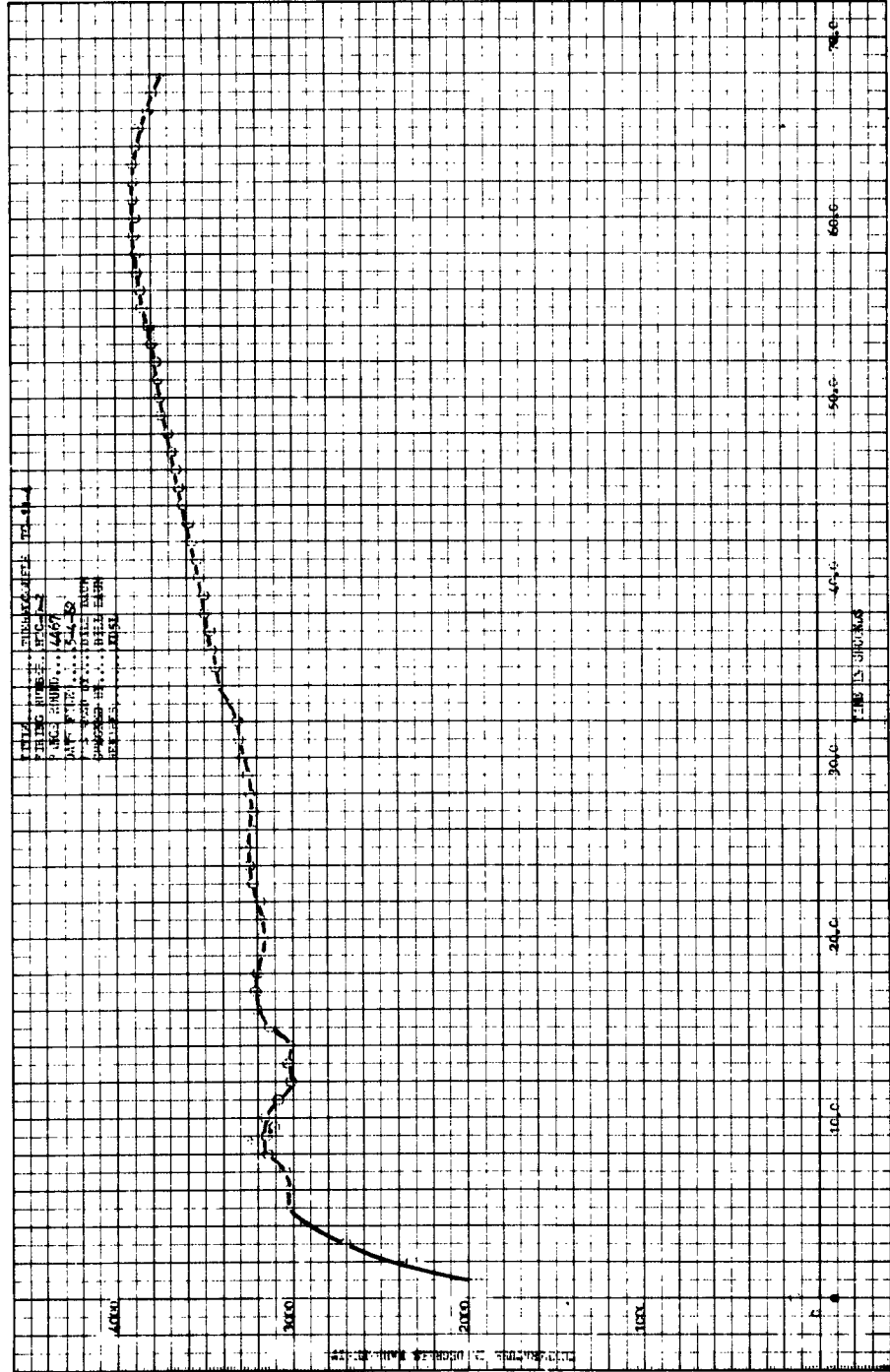


Figure 29 Temperature Plot, TC 11-4



Figure 30 Temperature Plot, TC 11-5

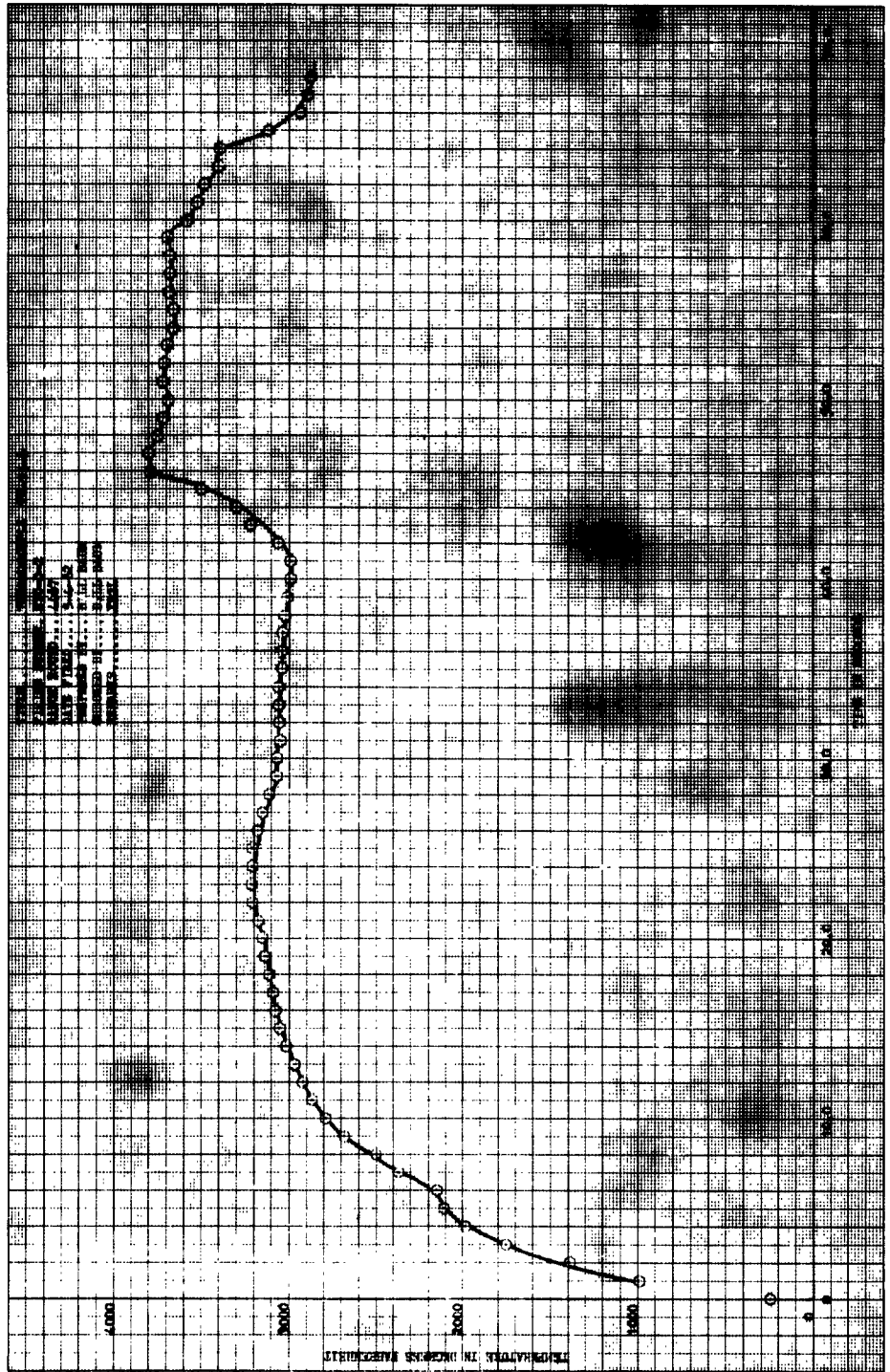


Figure 31 Temperature Plot, TC 11-6



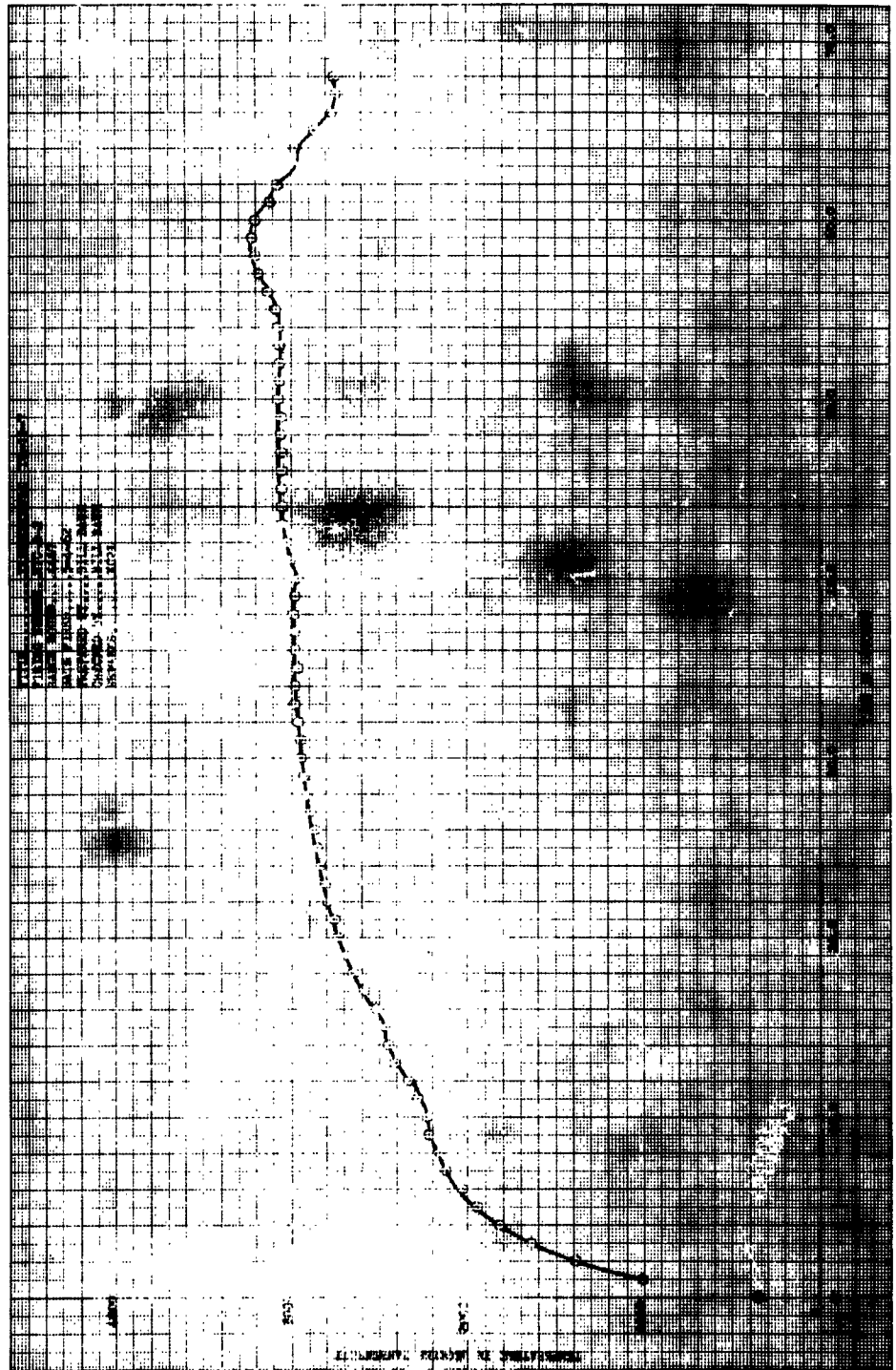


Figure 32 Temperature Plot, TC 11-7

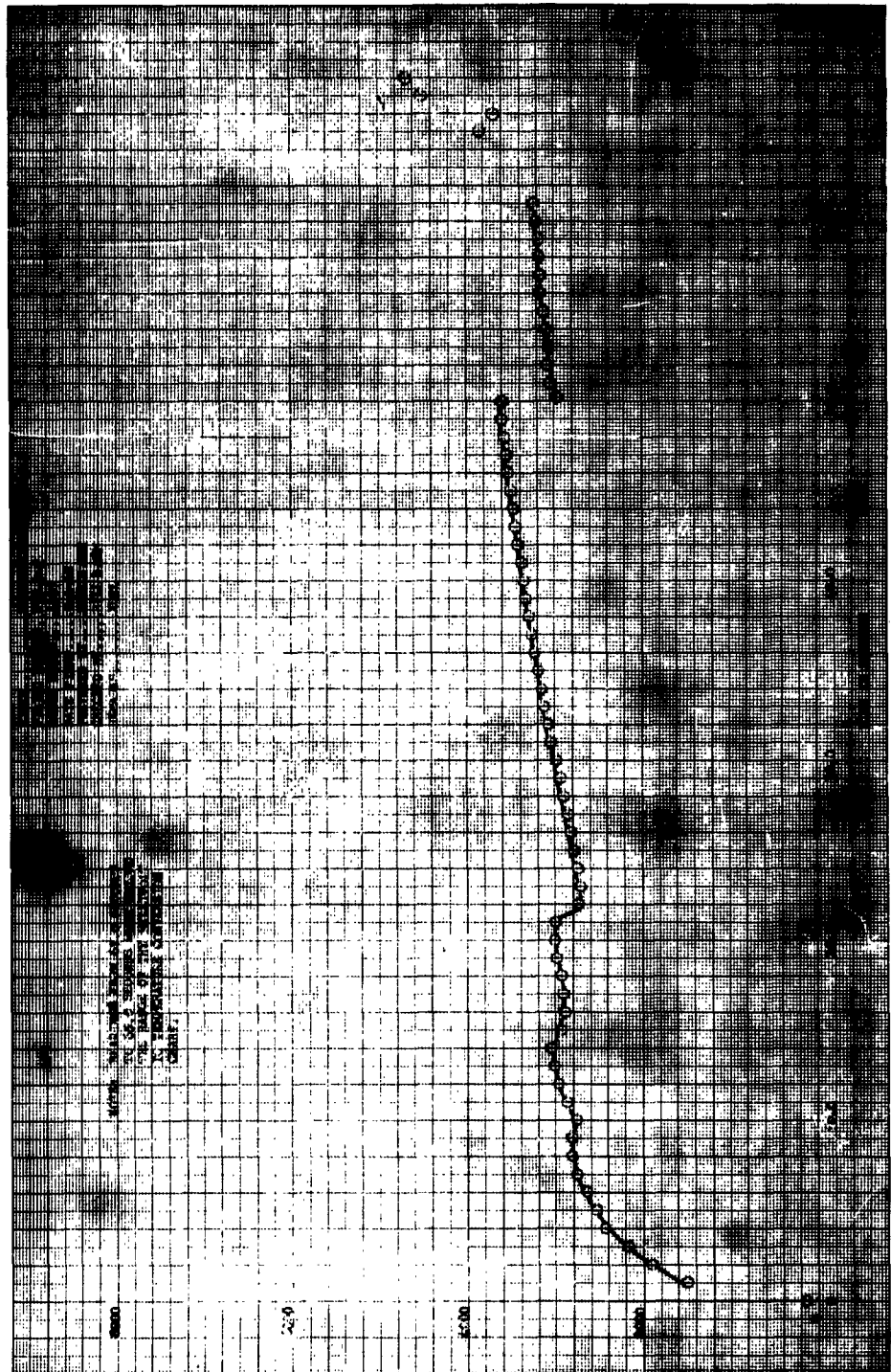




Figure 34 Temperature Plot, TC 11-9

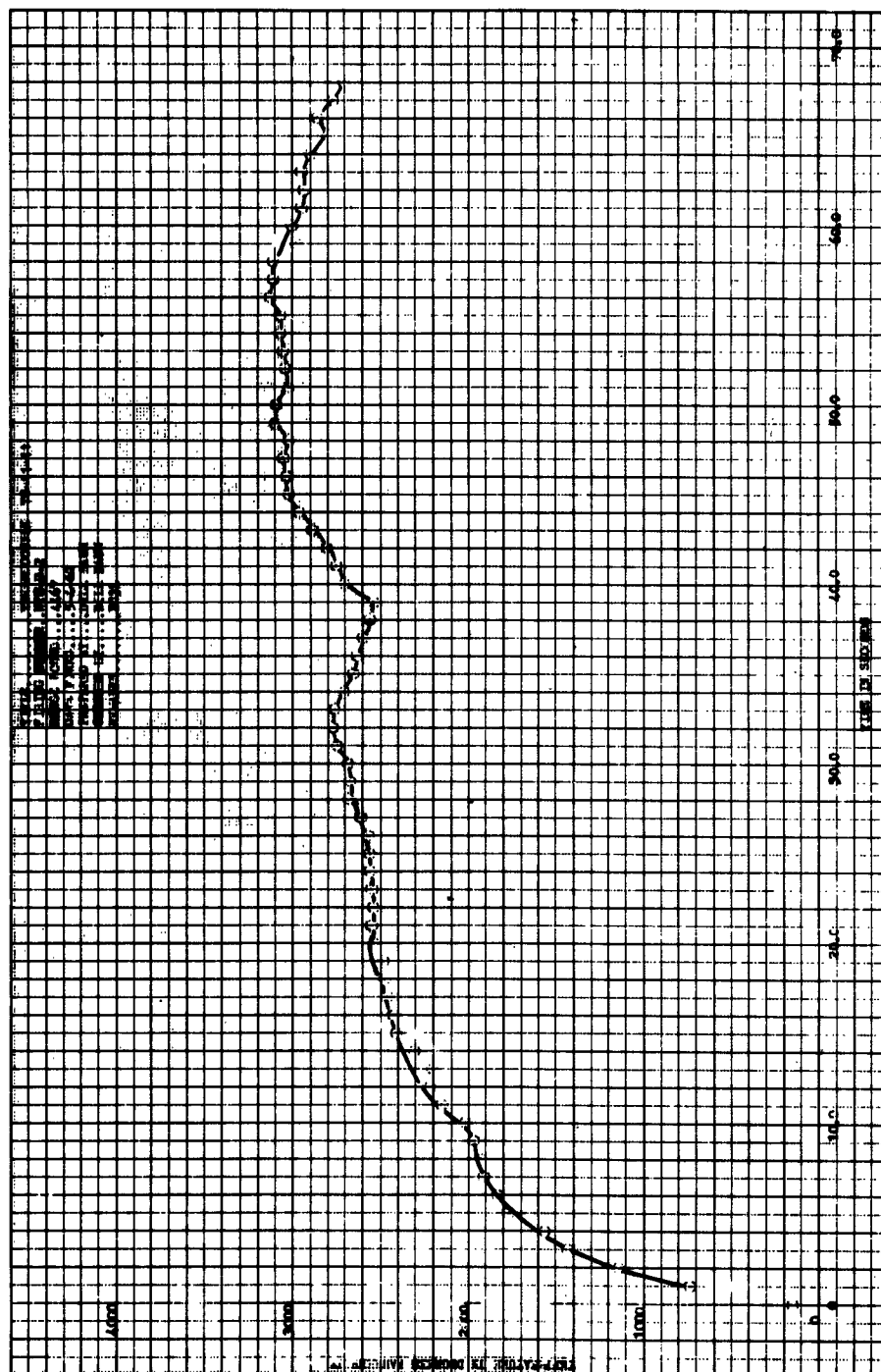


Figure 35 Temperature Plot, TC 11-11



Figure 36 Temperature Plot, TC 51



Figure 37 Temperature Plot, TC 52

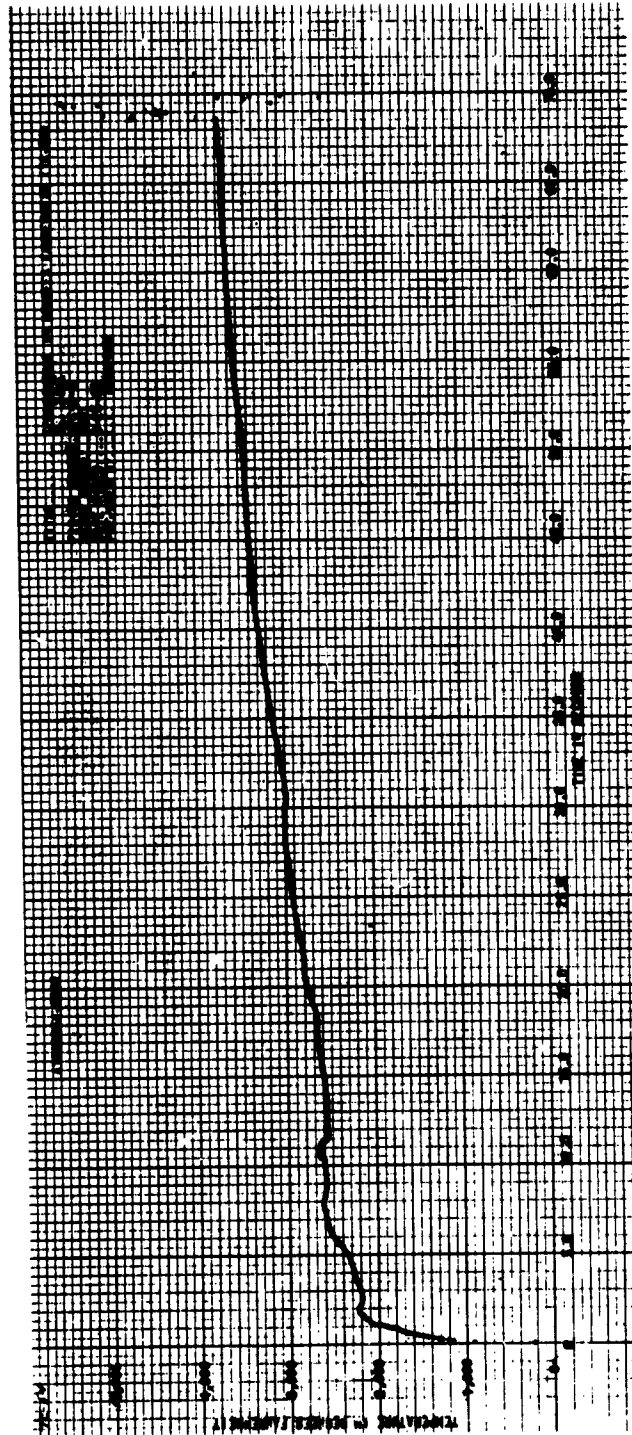


Figure 38 Temperature Plot, TC 54

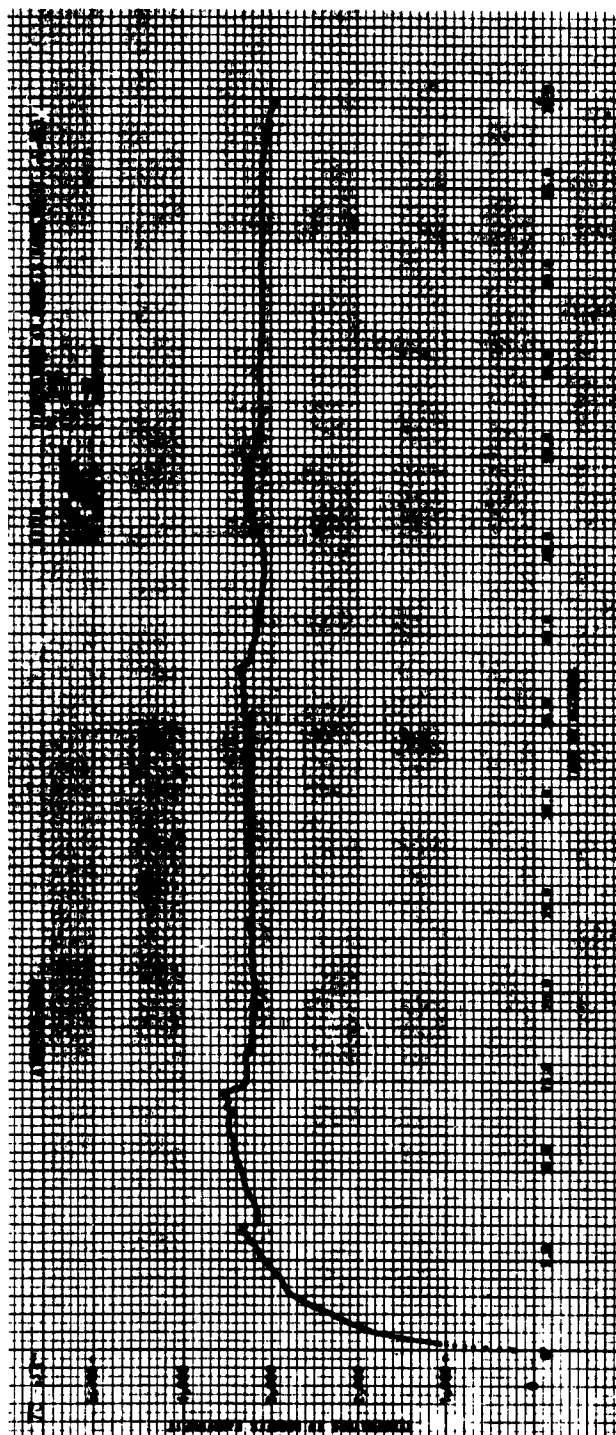


Figure 39 Temperature Plot, TC 55



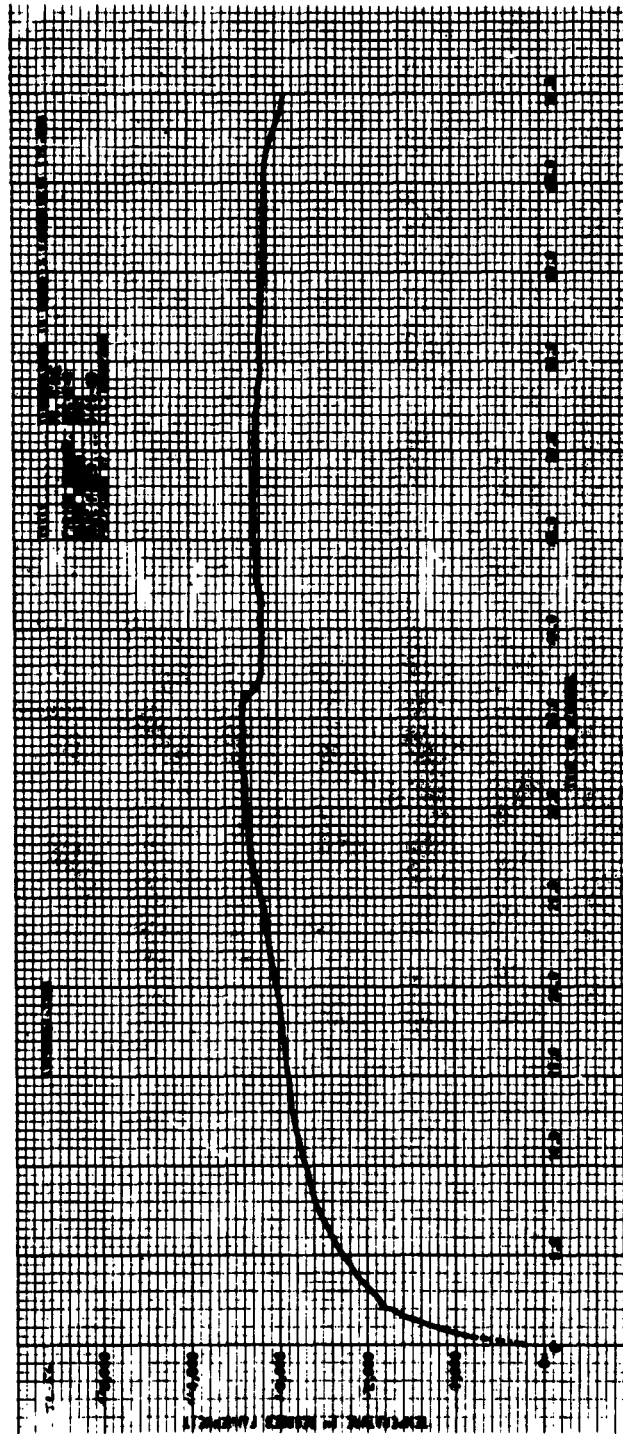


Figure 40 Temperature Plot, TC 56

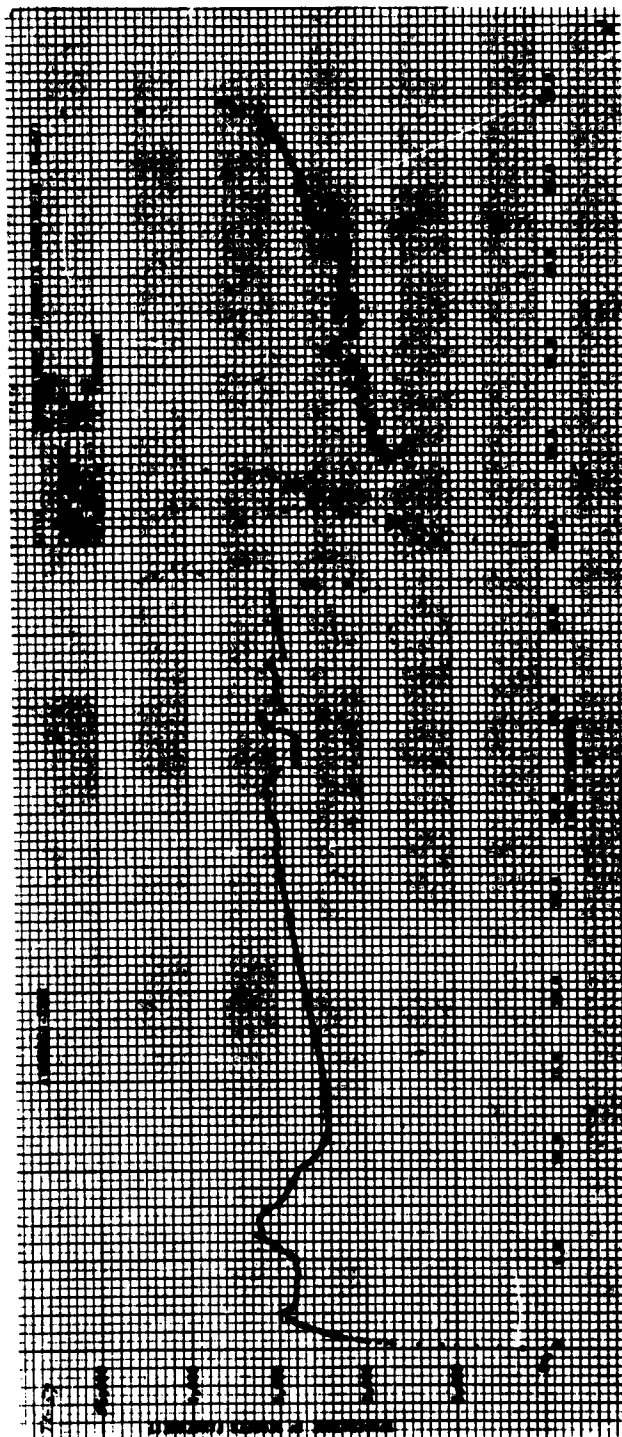


Figure 41 Temperature Plot, TC 57

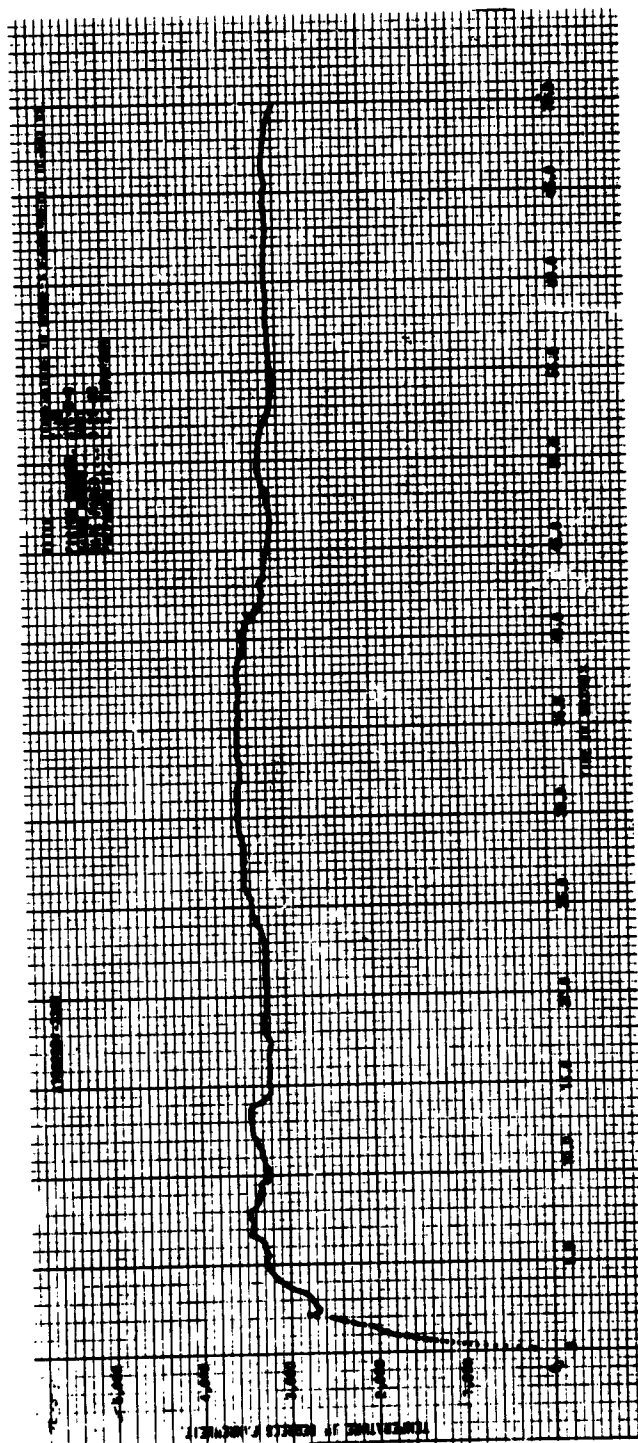


Figure 42 Temperature Plot, TC 58



Figure 43 Temperature Plot, TC 59



Figure 44 Temperature Plot, TC 60

# I

## LIST OF REFERENCES

1. "Physical Properties of Graphite, Carbon, ANI and ARRI," J. G. Lewis, American Metal Products Company, Engineering Science Division, Ann Arbor, Mich.
  2. "Physical Properties of R/M Style 150-RPD Molding Compound," Raybestos - Manhattan Co., Manheim, Pa., Tech. Data RPD-8B, 1 January 1961.
  3. "Progress Report for June 1961 to 1 October 1961," Submitted to Hercules Powder Company, Bacchus, Utah by High Temperature Materials, Inc., Boston, Mass., 26 October 1961.
  4. "A Simple Equation for Rapid Estimation of Rocket Nozzle Convection Heat Transfer Coefficients," D. R. Bartz Jet Propulsion, Vol. 27, No. 1, January 1957.
- # C

# DISTRIBUTION LIST

## A METHOD OF OBTAINING AN OVERALL HEAT TRANSFER FILM COEFFICIENT IN SOLID FUEL ROCKET NOZZLES

<u>Copies</u>	<u>Recipient</u>	<u>Mail Stop</u>
1	Hq. BSD (AFSC), Norton AFB; Attn: BSRPQ-1	
2	Hq. BSD (AFSC), Norton AFB; Attn: BSRPQ-2	
3 thru 5	STL, Norton AFB; Attn: Mr. J. R. McGibbeny	
6 thru 9	STL, Redondo Beach; Attn: Mr. R. L. Greengard	
10 thru 19	Armed Services Technical Information Agency, Arlington 12, Virginia	
20 thru 23	Central Intelligence Agency, Washington 25, D.C.	
24-25	National Aeronautics & Space Administration Washington 25, D.C.	
26	Rocket Propulsion Laboratory, Edwards; Attn: DOSMS	
27	Hq. OOAMA (OOYE), Hill AFB, Utah	
28	D. W. Austin/J. W. Kordig	504
29	D. E. Borgmeier	504
30	D. E. Boynton	100G2-1
31	B. Brown	507
32	J. W. Lindsey	117-T-48
33	A. H. Peterson	100G2-2
34	H. S. Heaton	507
35	K. B. Isom	507
36	J. R. Wilson/G. R. Duke	510
37-38	Publications Library	702
39 (repro)	Publications Library	702
40	Central File Library	509-C
	J. L. Morse (letter only)	502
	A. H. Nielson (letter only)	81-16-1
	M. Cohen, Philadelphia (letter only)	